Biomedicine & Pharmacotherapy 179 (2024) 117326

Contents lists available at ScienceDirect

Biomedicine & Pharmacotherapy

journal homepage: www.elsevier.com/locate/biopha

A cocktail of histidine, carnosine, cysteine and serine reduces adiposity and improves metabolic health and adipose tissue immunometabolic function in ovariectomized rats

Julio Baudin [a,b], Julia Hernandez-Baixauli [a,1], Jordi Romero-Giménez [a], Hong Yang [c], Francisca Mulero [d], Francesc Puiggròs [e], Adil Mardinoglu [c,f], Lluís Arola [b,*], Antoni Caimari [e,*]

[a] Eurecat, Centre Tecnològic de Catalunya, Technological Unit of Nutrition and Health, Reus 43204, Spain
[b] Nutrigenomics Research Group, Department of Biochemistry and Biotechnology, Universitat Rovira i Virgili, Tarragona 43007, Spain
[c] Science for Life Laboratory, KTH Royal Institute of Technology, Stockholm SE-17165, Sweden
[d] Molecular Imaging Unit, Spanish National Cancer Research Centre (CNIO), Madrid, Spain
[e] Eurecat, Centre Tecnològic de Catalunya, Biotechnology Area, Reus 43204, Spain
[f] Centre for Host-Microbiome Interactions, Faculty of Dentistry, Oral & Craniofacial Sciences, King's College London, London, United Kingdom

ARTICLE INFO

Keywords:
Histidine
Serine
Carnosine
Cysteine
Menopause
Obesity
Immunometabolic health
Nutraceuticals
Complementary and alternative therapies

ABSTRACT

Many women have sought alternative therapies to address menopause. Recently, a multi-ingredient supplement (MIS) containing L-histidine, L-carnosine, L-serine, and L-cysteine has been shown to be effective at ameliorating hepatic steatosis (HS) in ovariectomized (OVX) rats, a postmenopausal oestrogen deficiency model. Considering that HS frequently accompanies obesity, which often occurs during menopause, we aimed to investigate the effects of this MIS for 8 weeks in OVX rats. Twenty OVX rats were orally supplemented with either MIS (OVX-MIS) or vehicle (OVX). Ten OVX rats received vehicle orally along with subcutaneous injections of 17β-oestradiol (OVX-E2), whereas 10 rats underwent a sham operation and received oral and injected vehicles (control group). MIS consumption partly counteracted the fat mass accretion observed in OVX animals, leading to decreased total fat mass, adiposity index and retroperitoneal white adipose tissue (RWAT) adipocyte hypertrophy. OVX-MIS rats also displayed increased lean mass and lean/fat ratio, suggesting a healthier body composition, similar to the results reported for OVX-E2 animals. MIS consumption decreased the circulating levels of the proinflammatory marker CRP, the total cholesterol-to-HDL-cholesterol ratio and the leptin-to-adiponectin ratio, a biomarker of diabetes risk and metabolic syndrome. RWAT transcriptomics indicated that MIS favourably regulated genes involved in adipocyte structure and morphology, cell fate determination and differentiation, glucose/insulin homeostasis, inflammation, response to stress and oxidative phosphorylation, which may be mechanisms underlying the beneficial effects described for OVX-MIS rats. Our results pave the way for using this MIS formulation to improve the body composition and immunometabolic health of menopausal women.

Abbreviations: μCT, three-dimensional microcomputed tomography; 17β-E2, 17β-oestradiol; 8-OHdG, 8-hydroxy-2'-deoxyguanosine; ANOVA, analysis of variance; ATMs, adipose tissue macrophages; BMC, bone mineral content; BMD, bone mineral density; CRP, C-reactive protein; CT, central zone time spent; CTX-1, carboxy-terminal telopeptide of type I collagen; CVD, cardiovascular diseases; DGE, differential gene expression; EAE, enclosed arms entries; EAT, enclosed arms time spent; ECM, extracellular matrix; EE, energy expenditure; EPM, elevated plus maze; ER, oestrogen receptor; FDR, false discovery rate; GSH, glutathione; GSSG, oxidized glutathione; HDL-c., high-density lipoprotein cholesterol.; HOMA-IR, homeostasis model assessment-estimated insulin resistance; HRT, hormone replacement therapy; IR, insulin resistance; IWAT, inguinal white adipose tissue; KEGG, Kyoto Encyclopaedia of Genes and Genomes; LAR, leptin-to-adiponectin ratio; MCP-1, monocyte chemoattractant protein-1; MetS, metabolic syndrome; MIS, multi-ingredient supplementation; MWAT, mesenteric white adipose tissue; NAFLD, nonalcoholic fatty liver disease; NGS, next-generation sequencing; Non-HDL-c, high-density lipoprotein cholesterol; OAE, open arm entries; OAT, time spent in open arms; OC, osteocalcin; OVX, ovariectomized rats; PINP, procollagen I amino-terminal propeptide; RIN, RNA integrity number; RQ, respiratory quotient; R-QUICKI, revised quantitative insulin sensitivity check index; RWAT, retroperitoneal white adipose tissue; SHAM, sham-operated rats; TC, total cholesterol; TC/HDL-c, total cholesterol-to-high-density lipoprotein cholesterol ratio; TMC, tissue mineral content; TMD, tissue mineral density.

* Corresponding authors.
E-mail addresses: lluis.arola@urv.cat (L. Arola), antoni.caimari@eurecat.org (A. Caimari).
[1] Present address: Laboratory of Metabolism and Obesity, Vall d'Hebron-Institut de Recerca, Universitat Autònoma de Barcelona, Barcelona, Spain.

https://doi.org/10.1016/j.biopha.2024.117326
Received 16 May 2024; Received in revised form 13 August 2024; Accepted 21 August 2024
Available online 28 August 2024

1. Introduction

Menopause is a biological stage in a woman's life, marking the end of her reproductive years. It is characterized by the permanent cessation of menstrual cycles due to the loss of ovarian function. This loss leads to a decline in oestrogen production, which begins during the menopausal transition and becomes more pronounced in the postmenopausal state [1]. This reproductive ageing process can boost the appearance of different vasomotor symptoms, including sleep disturbances, night sweats and hot flashes [2,3]. In addition, menopause can trigger osteoporosis [4], decreased muscle mass content [4–6] and body weight gain accompanied by a shift in body fat distribution from a gynoid to an android pattern, contributing to increased abdominal fat accumulation [4–6]. Fat accretion may increase oxidative stress and low-grade inflammation and may trigger the development of metabolic disorders, such as hypertension, dyslipidaemia and insulin resistance (IR), thereby increasing the risk of cardiovascular diseases (CVD) [7–9]. Notably, both the risks of osteoporosis and CVD increase with age, and CVD is one of the most prominent causes of death worldwide, accounting for 47 % of deaths among women [10].

Hormone replacement therapy (HRT) is a widely prescribed solution for alleviating symptoms and ameliorating metabolic alterations associated with the postmenopausal state. However, the benefits and risks of HRT have been a matter of debate due to the unexpected findings obtained in 2002 in the Women's Ischaemia Syndrome Evaluation (WISE) study, which reported increased risks of suffering from CVD and endometrial and breast cancers for certain HRT treatments [11]. Currently, the safety and main side effects of this treatment depend on variables such as the type of HRT, treatment duration, and age at which the HRT begins after the final menstrual cycle. Remarkably, the safety and benefits of HRT appear to surpass the risks when it is prescribed to healthy women under 60 years of age or within the first ten years of amenorrhea [11]. While HRT effectively reduces vasomotor symptoms and osteoporosis, this treatment is less effective at reducing body weight gain and the risk of CVD (blood clots, stroke, thromboembolism and coronary heart disease) and at ameliorating affective disorders such as Alzheimer's disease and dementia. Moreover, HRT is not advised for women with a medical history of endometrial or breast cancer [11].

In recent years, the controversy about the risks associated with HRT has prompted many women to look for alternative therapies to address menopause, promoting the emergence of alternative approaches such as natural extracts, bioactive compounds and nutraceuticals to ameliorate vasomotor symptoms and metabolic disturbances related to menopause. Among them, isoflavones derived from soy, commonly known as phytoestrogens, are well-researched natural bioactive compounds with beneficial effects on menopause-related alterations. Genistein, the most abundant isoflavone in soy, accounts for 60 % of total isoflavones and exhibits twenty-fold greater selectivity for oestrogen receptor (ER) β than for ERα. This selectivity is advantageous because most side effects are associated with binding to ERα [12]. However, the biological activity of phytoestrogens varies among individuals because their activity depends on the metabolism of these precursors into more active compounds, which requires the activity of specific intestinal bacteria and hepatic enzymes, and both processes involve well-described interindividual variations. For instance, only the isoflavonoid daidzein is converted into its most bioactive and absorbable isoform, equol daidzein, by approximately 30 % of the population [13].

In a very recent study, members of this current team showed that, in ovariectomized (OVX) rats, a postmenopausal model with oestrogen deficiency, the combined consumption of the bioactive compounds hesperidin, phytosterols and curcumin effectively reduced obesity and improved metabolism-related alterations to a very similar extent to those observed in response to subcutaneous injections of 17β-oestradiol (17β-E2), a treatment that resembles one of the HRTs administered to menopausal women [14]. Specifically, this multi-ingredient supplement (MIS) significantly decreased the total fat mass content; the weights of mesenteric (MWAT), retroperitoneal (RWAT) and inguinal (IWAT) white adipose tissue depots; and the adiposity index in addition to increasing the total lean mass content and the lean/fat mass ratio, clearly indicating an improvement in body composition. In addition, MIS consumption decreased the circulating leptin levels and increased the level of the surrogate marker of insulin sensitivity, R-QUICKI, as well as the adiponectin-to-leptin ratio, which has been described in humans as a predictive and reliable biomarker for adipose tissue inflammation and the cardiometabolic risk associated with obesity [15]. These findings paved the way to promote the use of this MIS as an alternative therapy to ameliorate obesity and to improve the cardiometabolic health of menopausal women and were consistent with our idea that combined supplementation with different bioactive compounds that act against complementary targets is a suitable strategy to ameliorate cardiometabolic risk factors, as was previously documented in different studies, including some performed by the authors of the present work [16–19]. Similarly, members of our group have consistently reported a significant decrease in the circulating level of histidine in patients with morbid obesity as the severity of nonalcoholic fatty liver disease (NAFLD) increases [19] and based on these findings, we hypothesized that the consumption of a blend of amino acid-related compounds, including histidine, serine, cysteine and carnosine (β-alanyl-L-histidine dipeptide), could be an effective therapy for ameliorating NAFLD because (i) histidine is an essential amino acid that needs to be obtained from the diet; (ii) carnosine is a histidine-containing dipeptide and, therefore, can increase histidine levels; (iii) cysteine is an inhibitor of the histidine catabolizing enzyme ammonia lyase; (iv) serine is a precursor of cysteine; and (v) one of the main hallmarks of NAFLD is oxidative stress, and serine and cysteine may increase the cellular levels of glutathione (GSH), the most abundant endogenous antioxidant. This hypothesis was validated in both diet-induced and genetic leptin-deficient *ob/ob* mouse models and in OVX rats, which displayed decreased hepatic steatosis after the consumption of this amino acid-related MIS [19]. Considering our previous results concerning the reported beneficial effects on hepatic steatosis in OVX rats, that NAFLD is a metabolic disorder that frequently accompanies obesity and metabolic syndrome (MetS) [20], that different studies performed mainly in rodents but also in humans have shown that supplementation with carnosine [21,22], serine [23,24], cysteine [25,26] and especially histidine [27–31] can ameliorate obesity, promote glycaemic control, and ameliorate IR, inflammation or oxidative stress, in the present study, we hypothesized that this amino acid-related MIS would also be an effective approach for ameliorating obesity and metabolism-related alterations that can occur during the postmenopausal period.

Menopausal women can present increased risks of suffering cognitive impairment, anxiety and depression [32]. Some preclinical studies have shown that histidine intake increases the levels of histamine in the brain, improving learning and memory impairments [33,34] and reducing anxiety-like behaviours [35,36]. Furthermore, different preclinical and clinical studies have shown that carnosine supplementation ameliorates cognitive decline in animal models of Alzheimer's disease, in elderly individuals and in subjects with mild cognitive decline [21]. In addition, some studies performed with rodents [37,38] and one clinical study [39] suggested that carnosine has beneficial effects on anxiety, stress and depression-like behaviours. On the other hand, significant associations between lower levels of cysteine and a lower bone mineral density (BMD) [40] and higher levels of the bone turnover marker carboxy-terminal telopeptide of type I collagen (CTX-1) were found in postmenopausal women [41], suggesting an important role for this semiessential amino acid in bone metabolism. This idea was reinforced by the fact that cysteine supplementation for 8 weeks counteracted the loss of BMD in OVX mice, showing effects similar to those observed after 17β-E2 injections [42].

The main aim of the present study was to evaluate whether oral intake of an MIS including L-histidine, L-carnosine, L-serine and L-cysteine for 8 weeks would exert beneficial effects on fat mass accretion

and cardiometabolic risk factors related to the postmenopausal state in an OVX rat model and to explore the underlying mechanisms involved. In this work, we also aimed to investigate the effects of the chronic administration of the MIS on bone and behavioural-related parameters to provide insights into the potential of this amino acid-related MIS to ameliorate the multifactorial alterations that can occur during menopause. The effects of this MIS were compared to those of subcutaneous injections of 17β-E2, an agent that resembles HRT.

2. Materials & methods

2.1. Ingredients

L-Histidine base (HIS; Ref.: AMI-019) and L-Cysteine (CYS; Ref.: AMI-011) were purchased from NUTRIFOODS S.L.U. (Barcelona, Spain). According to the supplier, the products were 99.6 % and 99.7 % pure, respectively. L- Carnosine 98 % (CAR; 208170250) was purchased from Thermo Fischer Scientific (Massachusetts, USA). L-Serine (SER; Ref.: S4500) was purchased from Merck KGaA (Frankfurt, Germany).

2.2. Animals, diet and treatments

The Animal Ethics Committee of the Technological Unit of Nutrition and Health of EURECAT (Reus, Spain) and the Generalitat de Catalunya approved all procedures (protocol code 11223). The study followed the 'Principles of Laboratory Animal Care', complied with the ARRIVE guidelines and was conducted in compliance with the EU Directive 2010/63/EU for animal experiments. The rodents used in this research consisted of forty 24-week-old female Sprague—Dawley rats (JANVIER LABS, Saint-Berthevin, France). Thirty rats were bilaterally ovariectomized (OVX), and 10 rats underwent a sham operation (SHAM) at the JANVIER facility. Before they arrived at the animal facility of Eurecat, the 40 animals were fed a maintenance rodent chow diet for 1 week to stabilize them because of ovariectomy surgery before shipment at the age of 25 weeks. Throughout the study, all rats were housed in pairs at 22 °C on a 12 h light/dark cycle with lights on at 9:00 am, and they had ad libitum access to food and water. After an acclimatization period of 1 week, the 30 OVX rats were divided into three experimental groups based on the treatment they received for 8 weeks (OVX, OVX-E2, and OVX-MIS; n=10 rats per group), and the 10 sham-operated (SHAM; n=10) rats were assigned to the control group. OVX-MIS animals were supplemented daily for 8 weeks with an MIS that included four amino acid-related compounds at the following doses per body weight: L-histidine, carnosine and L-serine at 105 mg/kg and L-cysteine at 245 mg/kg. The dosages were obtained by extrapolating the doses used by our group for mice in a previous study [19]. Considering the Reagan–Shaw formula, the doses of histidine, carnosine, and serine used were equivalent to the daily consumption of 1022 mg of these compounds for a 60-kg human [43]. For cysteine, the extrapolated daily intake using the same formula was 2384 mg. For each compound, these dosages are considered acceptable, well tolerated and safe in the context of nutraceutical supplementation [27,44–46]. The amino acid-related compounds were dissolved in peach juice enriched with 45.71 mg/mL fructose along with an acid taste masker (AROMA ACTI'MASK PRO, [E414 or gum Arabic]; Metarom Ibérica S.A., Barcelona, Spain) at 10 mg/mL to ensure voluntary consumption and minimize the stress of the animals. The SHAM, OVX and OVX-E2 groups were supplemented daily with peach juice + fructose at 45.71 mg/mL (vehicle) for 8 weeks. Half of the daily treatment was administered orally via a syringe of 1 mL in a volume of 0.3–0.4 mL between 09:00 and 10:00 am, and the other half was administered via the same protocol between 12:00 and 1:00 pm to guarantee the full voluntary consumption of the treatments. Four days before the beginning of the treatments, the rats were trained to lick peach juice (0.3 mL) to ensure voluntary consumption. OVX-E2 rats also received biweekly subcutaneous injections of 25 μg/kg body weight 17β-E2 (Sigma—Aldrich, St. Louis, MO) in a carrier solution of corn oil, whereas the remaining groups received the same dose of the vehicle (corn oil). All groups were fed a standard chow diet (Teklad Global 14 % Protein Rodent Diet or February 2024, Harlan, Barcelona, Spain). The caloric breakdown of the diet (2.9 kcal/g) was 20 % protein, 13 % fat, and 67 % carbohydrates. Body weight was recorded once each week, food was renewed daily, and food intake was documented every 7 days.

For urine collection, which was performed at the 8th week of the study, rats were food deprived for 3 hours (from 8:00 am to 11:00 am) with access to water. Afterward, rats were housed individually in a square cage with an adequate amount of hydrophobic sand (LabSand®, Coastline Global, CA, USA) to cover the bottom of the cage. Animals were food and water deprived for the duration of the urine collection (5 hours). Urine drops were collected with a pipette every hour and transferred into a polypropylene tube with a cap, which was stored at 4 ºC. And the end of the period all the urine aliquots collected were pooled and stored at −80 ºC until further analyses.

On Day 57, the rats were sacrificed by decapitation after 6 h of diurnal fasting and without receiving any treatment. Blood samples were collected in heparinized tubes, and plasma was obtained by centrifugation and stored at −70 °C until further analysis. The liver, caecum, kidneys, gastrocnemius and soleus muscles, the left femur and tibia, and the RWAT, MWAT and IWAT depots were rapidly removed, weighed, frozen in liquid nitrogen and stored at −70 °C until further analysis. The right femur and tibia were also collected, immersed in 70 % ethanol and stored at room temperature until the three-dimensional microcomputed tomography analysis.

2.3. Body composition analyses

An EchoMRI-700™ device (Echo Medical Systems, L.L.C., Houston, TX, USA) was used to evaluate the relative lean and fat mass contents of the rats without anaesthesia on Days 1, 30 and 57. The analyses were performed in triplicate at 8:00 am under ad libitum conditions, and the results are presented as a percentage of body weight. Fat mass and lean mass weights (%) were calculated according to the formula (100* fat or lean/body weight) and are presented as a percentage of body weight. The lean/fat mass ratio was calculated as the lean mass divided by the fat mass.

2.4. Adiposity index

The adiposity index was calculated as the sum of the weights of the IWAT, MWAT and RWAT depots (in grams) for each rat and was reported as a percentage of body weight.

2.5. The homeostasis model assessment-estimated insulin resistance (HOMA-IR) analysis

The HOMA-IR, a surrogate marker of IR, was calculated with the following formula: (fasting glucose level –mmol/L- × fasting insulin level-μU/mL-)/22.5 [47].

2.6. Plasma analysis

An enzymatic colorimetric kit was used to determine plasma glucose levels (992330/QCA, Barcelona, Spain). The circulating levels of total cholesterol (TC) and high-density lipoprotein cholesterol (HDL-c) were measured using reflectance spectrophotometry with the Vitros® 5600 Integrated System (QuidelOrtho Corporation, San Diego, CA, USA). The non-high-density lipoprotein cholesterol (non-HDL-c) level was calculated by subtracting the HDL cholesterol concentration from the TC concentration. The TC/HDL-c ratio was calculated as the TC level divided by the HDL-c level. Circulating insulin levels were measured using a rat/mouse ELISA kit (10–1250–01/MERCODIA, Upssala, Sweden). Plasma leptin levels were determined with a rat ELISA kit (EZRL-83 K/Millipore, Barcelona, Spain), and the circulating levels of

adiponectin were quantified using a rat total adiponectin/Acrp30 Quantikine ELISA Kit (RRP300/R&D systems, Minnesota, USA). The leptin-to-adiponectin ratio (LAR) was calculated as the circulating levels of leptin divided by the circulating levels of adiponectin. This ratio is considered a good predictor of type 2 diabetes and MetS [48]. The levels of the inflammatory markers monocyte chemoattractant protein-1 (MCP-1) and C-reactive protein (CRP) were quantified in plasma using the BMS631INST and the ERCRP ELISA kits, respectively (INVITROGEN, Massachusetts, USA). The circulating levels of the biomarkers of bone turnover, procollagen I amino-terminal propeptide (PINP), osteocalcin (OC) and CTX-1, were measured using PINP ELISA kit (AC-33F1, IDS, UK), osteocalcin ELISA kit (AC-12F1, IDS, UK) and CTX ELISA kit (AC-06F1, IDS, UK).

2.7. Urine analysis

A commercial ELISA kit was used to quantify the levels of 8-hydroxy-2'-deoxyguanosine (8-OHdG) (STA-320/CELL BIOLABS INC. Chicago, USA) in urine. The levels of this metabolite were normalized to the creatinine levels, which were analysed using the Creatinine Urinary Detection Kit (EIACUN/Thermo Fischer Scientific, Massachusetts, USA).

2.8. Analysis of total, oxidized and reduced glutathione levels in the liver

Liver samples were used to quantify the levels of total GSH, reduced GSH, and oxidized GSH (GSSG) using the Glutathione Colorimetric Detection Kit from EIAGSHC/INVITROGEN (Massachusetts, USA). The results are presented in μmol per g of hepatic protein, which was calculated using the BCA assay method. The GSSG/GSH ratio was calculated as the oxidized GSH level divided by the reduced GSH level.

2.9. Histological analysis

Buffered formalin (4 % formaldehyde, 4 g/L NaH2PO4, 6.5 g/L Na2HPO4; pH 6.8) was used to preserve fixed portions of RWAT (n = 8 per group), which were cut at a thickness of 5 μm and stained with haematoxylin & eosin (H&E). An ECLIPSE microscope (ECLIPSE Ti; Nikon, Tokyo, Japan) coupled to a digital sight camera (DS-Ri1, Nikon) was used to obtain the RWAT images (magnification 100×). Image analyses were performed using ImageJ NDPI software (National Institutes of Health, Bethesda, MD, USA; https://imagej.nih.gov/ij, accessed on 22 March 2024, version 1.54 g). The AdipoSoft plugin was used to quantify the adipocyte area in the RWAT sections from the different groups.

2.10. Microcomputed tomography analyses

The bone composition of the right tibia and femur was determined postmortem in fixed samples by performing three-dimensional micro-computed tomography (μCT) analysis, as previously described [14]. The tissue mineral content (TMC), bone mineral content (BMC), tissue mineral density (TMD) and BMD values were quantified from μCT scans using GE MicroView software v2.2.

2.11. Indirect calorimetry

The Oxylet Pro™ System (PANLAB, Cornellà, Spain) was used to perform indirect calorimetry analyses of the different groups between Days 29 and 33 after the beginning of the treatments, throughout 22 h (from 11:00 am to 09:00 am), under ad libitum conditions and with free access to water. At 09:00 am, the animals received the corresponding treatment and were transferred from their cages to an acrylic box (Oxylet LE 1305 Physiocage, PANLAB). After an initial acclimatization period of 2 h, the respiratory quotient (RQ), the fat and carbohydrate oxidation rates and the energy expenditure (EE) were calculated as previously described [49].

2.12. Behavioural evaluation

2.12.1. Elevated plus maze (EPM)—anxiety-like behaviour

The animals were tested in the EPM [50] on Day 36 to evaluate anxiety-like behaviour. The EPM test apparatus consisted of four arms, two open arms (45 cm long × 10 cm wide) and two enclosed arms with walls (45 cm long × 10 cm wide × 35 cm height), which were positioned alternatively and extended from a 10 cm square, common central platform positioned 90° from each other to form the shape of a plus sign. The apparatus was elevated 50 cm above the floor. The rat was placed in the centre of the maze (always facing the same closed arm), and videos of the EPM test were recorded for five minutes (300 s) using a tracking system (ANY-Maze, version 4.82, SD Instruments, US) and analysed to score the distance travelled, time spent and the number of entries into each arm. The apparatus was wiped clean with 70 % ethanol before each animal was tested. Behavioural measures were defined according to previous studies [51] and included the following: the frequency of open and enclosed arm entries (OAEs and EAEs), defined as all four paws placed inside an arm; total arm entries; and total time spent in the open (OAT) and enclosed arms (EAT) and in the central area (CT). These data were used to calculate the percentage of OAEs [% OAEs; (open entries/open + enclosed entries) × 100], the percentage of EAEs [% EAEs; (enclosed entries/open + enclosed entries) × 100], the percentage of OAT [%OAT; (time in open arms/300) × 100], the percentage of EAT [% EAT; (time in enclosed arms/300) × 100] and the percentage of CT [% CT; (time in central zone/300) × 100]. Behaviour in the open arms is indicative of anxiety in the animal, with a large amount of time and entries into the open arms indicating low anxiety [52], while the distance travelled in the enclosed arms is considered a measure of locomotion [53].

2.12.2. Y-maze test—spatial reference memory

The rodents were subjected to the Y-Maze [54] test on Day 40 to assess spatial reference memory. This equipment is composed of three identical arms (45 cm long × 10 cm wide × 25 cm (walls) tall) that are symmetrically placed at an angle of 120° to each other to form a Y shape. This assessment consisted of a habituation phase and a test phase. In the habituation phase, the rats were placed at the end of one of the arms ("start arm") facing the wall. The rats were allowed to explore two arms of the Y-maze for five minutes (300 s), while entry into the third arm was blocked. The blocked arm was arranged alternately to mitigate potential bias. After the habituation phase, the rats were returned to their home cage for a 1 h intertrial interval. During the test phase, the rats were allowed to explore all 3 arms of the maze (including the novel third arm, which was previously blocked) for 5 minutes (300 s). The apparatus was wiped clean with 70 % ethanol before the habituation and test phases of each animal. The time and number of entries into the novel arm were analysed using a tracking system (ANY-Maze, version 4.82), and the number of alternations was calculated as the number of entries into three different arms in succession. These data were used to calculate the percentage of entries in the novel arm (number of entries in the novel arm/total number of entries × 100), the novel arm preference index (%) using the formula [(time in novel arm/300) × 100] and the spontaneous alternation (%) with the following formula: {[number of alternations/(total number of arm entries - 2)] × 100} [34]. This test is based on the natural drive due to the innate curiosity of rodents to explore novel environments, and a rat with no preference for any of the arms during the testing session is classified as having poor spatial memory [54].

2.13. Transcriptomic and gene set enrichment analyses

The transcriptomic analysis was performed on RNA samples from the RWAT of rats in the OVX and OVX-MIS groups (n = 7 rats per group). Total RNA was extracted using Tripure Reagent (Roche Diagnostic, Barcelona, Spain) and purified with Qiagen RNeasy Mini Kit spin

columns (Izasa, Barcelona, Spain) according to the manufacturer's instructions, and RNA integrity was measured on an Agilent Bioanalyzer (Agilent Technologies, South Queensferry, UK). All samples had optimal quality parameters (RIN > 5) and were used for the construction of next-generation sequencing (NGS) libraries. The subsequent NGS libraries were converted to FASTQ format using Illumina NovaSeq 6000 in S4 flow cell mode (Illumina Way, California, USA). Gene abundance in all RNA-seq data (in both raw counts and transcripts per million) was processed using the Kallisto pipeline [55] based on the *Rattus norvegicus* genome from Ensembl release version 107. Kyoto Encyclopaedia of Genes and Genomes (KEGG) pathway analysis was performed using all the gene expression data and was carried out separately for distinctly upregulated, mixed-direction upregulated, mixed-direction downregulated and distinctly downregulated genes. The Benjamini–Hochberg false discovery rate (FDR) test was performed to manage false-positive outcomes. Only the pathways exhibiting an FDR-derived q-value less than 0.05 (*adj*. $p < 0.05$) were considered as enriched of pathways according to the R package Piano v2.16.0 (nperm=1000) [56]. R/Bioconductor package ComplexHeatmap v2.16.0 [57] was used to create a heatmap to visualize significantly regulated KEGG pathways (*adj*. $p < 0.05$) in OVX-MIS animals compared with their OVX counterparts. The differential gene expression (DGE) analysis was performed using the R/Bioconductor package DESeq2 v1.40.2 [55], and the Benjamini–Hochberg FDR test was performed to manage false-positive outcomes. Only the genes exhibiting an FDR-derived q-value less than 0.1 (*adj*. $p < 0.1$) were recognized as DGEs. The resulting gene lists were annotated and filtered for significantly differentially up- and downregulated genes (*adj*. $p < 0.1$ and log2(fold change) $> |0|$ or $< |-0|$, respectively). The log2(fold changes) for each gene were calculated using the R package Piano v2.16.0 (gene set statistic=reporter) [56]. Fold change values of the significant genes were calculated in Microsoft Excel from the log2(fold changes). The fold change equals the OVX-MIS/OVX ratio when the ratio increases or equals −1/ratio when the ratio decreases. The R package ggplot2 v3.4.4 [58] was used to create a volcano plot using all the gene expression data to visualize the expression pattern of the genes that significantly changed (*adj*. $p < 0.1$) between OVX and OVX-MIS animals. For the classification of the biological processes of the genes that were differentially expressed (*adj*. $p < 0.1$) between the OVX-MIS and OVX animals, we used only the "biological process" category of g:Profiler (g:GOst, https://biit.cs.ut.ee/gprofiler/gost, accessed on 17 February 2024, version e110_eg57_p18_4b54a898), which was applied to test functional enrichment analysis of significantly differentially expressed genes in biological process pathways [59]. Because the results of the whole genome array revealed that not all the significantly differentially expressed genes were identified by the KEGG pathway and g:Profiler programs, we supplemented the significantly enriched biological processes with nonannotated genes from the selected gene set using the scientific literature from biological databases (NCBI, PubMed and Human Protein Atlas, https://www.proteinatlas.org/, accessed on 4 March 2024). As processes overlapped, we consolidated them and assigned new names to better reflect their combined nature.

2.14. Statistical analyses

Statistical analyses were performed with IBM SPSS Statistics 28.0 (SPSS, IBM Corp. Armonk, New York, USA). Grubbs' test was used to detect outliers, which were discarded from further analysis. The assumption of normality was determined using the Kolmogorov—Smirnov test, and the homoscedasticity among groups was evaluated using Levene's test. When one or both of these conditions were not met, the data were transformed to the base-10 logarithm to obtain a normal distribution and/or similar variances before statistical testing. One-way ANOVA followed by Duncan's *post hoc* test (p value ≤ 0.05) were used to assess differences among the four groups in the variables analysed at one time point in the present study. The Welch test followed by the Games–Howell *post hoc* test were used when homoscedasticity was not assumed. The Kruskal—Wallis test followed by the Mann—Whitney U *post hoc* test were used as the nonparametric version of one-way ANOVA when the data did not follow a normal distribution. Differences among groups in the evolution of body weight (g), fat (%) and lean mass (%) on Days 1, 30 and 57 were analysed with repeated measures (RM-) ANOVA with time as a within-subject factor and intervention as a between-subject factor. When a significant interaction was found between both factors, one-way ANOVA followed by Duncan's *post hoc* test were used to determine intervention-related differences at each time point among groups. The data are presented as the means ± SEMs (n = 9–10). The level of statistical significance was set at bilateral 5 %.

3. Results

3.1. Effects of ovariectomy on body weight gain, fat accretion and metabolic-related alterations

At the beginning of the study, two weeks after surgery, the removal of the ovaries led to a greater baseline body weight in the OVX animals than in their SHAM counterparts (Table 1). At the end of the study, the OVX group displayed increased food intake (Table 1) and decreased EE (Supplementary Table 1) compared to the SHAM group. This finding could explain, at least in part, the greater body weight, body weight gain, fat mass percentage and fat mass gain observed at the end of the

Table 1
Cumulative food intake and biometric and plasma parameters in sham-operated (SHAM) and ovariectomized (OVX) rats after 8 weeks of intervention.

	SHAM	OVX	OVX-E2	OVX-MIS	Intervention effect (p value)
Cumulative Food Intake (g)	59.7 ± 0.4^{a}	73.4 ± 1.9^{b}	63.5 ± 2.7^{ac}	67.7 ± 1.7^{bc}	*I* (<0.001)
Biometric parameters					
Initial body weight (g)	338 ± 8^{a}	412 ± 4^{b}	407 ± 9^{b}	414 ± 6^{b}	*I* (<0.001)
Final body weight (g)	358 ± 7^{a}	472 ± 12^{b}	407 ± 15^{c}	455 ± 12^{b}	*I* (<0.001)
Liver (g)	9.8 ± 0.4	10.2 ± 0.3	10.0 ± 0.6	10.0 ± 0.2	NS (0.943)
Caecum (g)	5.15 ± 0.15	6.05 ± 0.45	5.26 ± 0.19	5.45 ± 0.37	NS (0.206)
Kidneys (g)	2.10 ± 0.07	1.96 ± 0.05	2.11 ± 0.10	1.98 ± 0.05	NS (0.348)
Gastrocnemius (g)	2.19 ± 0.09^{a}	2.57 ± 0.09^{b}	2.43 ± 0.10^{b}	2.65 ± 0.05^{b}	*I* (0.002)
Soleus (g)	0.190 ± 0.007	0.202 ± 0.011	0.210 ± 0.011	0.202 ± 0.009	NS (0.562)
Plasma parameters					
Glucose (mmol/L)	7.36 ± 0.30	7.77 ± 0.44	7.92 ± 0.15	7.83 ± 0.15	NS (0.343)
TC (mmol/L)	3.73 ± 0.30	4.05 ± 0.12	3.52 ± 0.14	4.07± 0.15	NS (0.153)
HDL-c (mmol/L)	2.79 ± 0.24	3.07 ± 0.16	2.96 ± 0.20	3.35± 0.11	NS (0.235)
Non-HDL-c (mmol/L)	0.94 ± 0.07^{a}	0.98 ± 0.12^{ab}	0.57 ± 0.10^{c}	0.73 ± 0.06^{bc}	*I* (0.009)
TC/HDL-c Ratio	1.35 ± 0.02^{a}	1.34 ± 0.06^{ab}	1.21 ± 0.04^{bc}	1.22 ± 0.01^{c}	*I* (0.001)

Data are presented as the means ± SEMs (n = 9–10). Different superscript lowercase letters (a, b, c) indicate significantly different mean values (one-way ANOVA and Duncan's *post hoc* test or Welch's test and Games–Howell *post hoc* test or Kruskal—Wallis test and Mann—Whitney U *post hoc* test, $p < 0.05$). *I*: the effect of the intervention. NS: nonsignificant differences. SHAM: sham-operated rats; OVX: ovariectomized rats; OVX-E2: OVX rats treated with 17β-oestradiol; OVX-MIS: OVX rats supplemented with the multi-ingredient; TC: total cholesterol; HDL-c: high-density lipoprotein cholesterol; Non-HDL-c: non-high-density lipoprotein cholesterol.

study in the OVX group than in the SHAM group (Table 1 and Fig. 1A-D). Consistent with the increased fat mass percentage observed in OVX rats, a significant increase in RWAT, MWAT and IWAT depots, as well as an increase in the adiposity index, were reported in these animals (Fig. 2A-D). Concurrently, the OVX group exhibited a lower final lean mass percentage, a greater loss of lean mass and a lower lean-to-fat ratio (Fig. 1E-G) than the SHAM group. Furthermore, untreated OVX animals displayed elevated circulating levels of leptin, adiponectin and insulin (Fig. 2E-G) in addition to increased HOMA-IR and LAR (Figs. 2H and 2I, respectively). Furthermore, according to the histological analyses of the RWAT, the removal of the ovaries also triggered adipocyte hypertrophy, increased the percentage of larger adipocytes and decreased the number of these cells in the OVX group (Fig. 3). OVX rats also displayed higher hepatic levels of oxidized GSH (GSSG) (Fig. 4F) than did their SHAM counterparts. Aside from the metabolic changes observed, OVX rats had a lower TMD in the right femur and a lower BMD and TMB in the right tibia than SHAM animals (Table 2). These results were accompanied by elevated circulating levels of the bone biomarkers of formation and resorption, OC and CTX-1, respectively (Table 2).

3.2. MIS and 17β-E2 treatments improved body composition and decreased adipocyte hypertrophy

17β-E2 administration significantly reduced the increase in body weight observed in the OVX group from Day 30 of intervention onwards (Fig. 1A) and fully counteracted the body weight gain at the end of the experimental period (Fig. 1B). These findings could be related, at least in part, to the lower food intake observed in the OVX-E2 group than in the OVX group (Table 1). OVX-MIS animals displayed slight decreases in body weight and body weight gain, although the differences compared with those in the OVX group were not statistically significant (Figs. 1A and 1B). This lack of significant effects of MIS consumption could be partly explained by the similar cumulative food intake observed between OVX-MIS rats and their OVX counterparts (Table 1). Compared with OVX animals, both the MIS group and the 17β-E2 injection group showed a significant progressive decrease in fat mass accretion, an effect that was statistically significant from Day 30 of intervention onwards (Fig. 1C). This result indicated a significant decrease in fat mass accumulation in both OVX-MIS and OVX-E2 rats (30 % and 69 % lower, respectively) (Fig. 1D). These findings are consistent with the significant decreases in RWAT weight (Fig. 2A) and adiposity index (26 % and 14 % lower in OVX-E2 and OVX-MIS rats, respectively) (Fig. 2D) observed in both groups of animals. Nevertheless, these antiadipogenic effects were more evident in the animals that received the 17β-E2 injections, which also displayed lower MWAT and IWAT weights than their OVX counterparts (Fig. 2B & 2 C, respectively).

Remarkably, both MIS and 17β-E2 injections effectively ameliorated the adipocyte hypertrophy observed in the RWAT of the OVX group to a similar extent (Fig. 3A). An inverse pattern was reported for the number of adipocytes, which was significantly lower in the OVX group than in the OVX-MIS and OVX-E2 groups (Fig. 3B). Consistent with these findings, representative RWAT histological images revealed larger adipocytes and fewer adipocytes in the OVX group (Fig. 3D) than in the OVX-E2 (Fig. 3E) and OVX-MIS (Fig. 3F) groups. Furthermore, the adipocyte size distribution revealed a decrease in the percentage of larger adipocytes and an increase in the percentage of smaller adipocytes in the RWAT of both OVX-MIS and OVX-E2 animals compared to those in the OVX rats, exhibiting a similar pattern to that observed in SHAM rats (Fig. 3G). In this study, we also investigated the impacts of the interventions on the lean mass content and body composition. Both OVX-MIS and OVX-E2 animals showed a greater lean mass content than their OVX counterparts from Day 30 onwards (Fig. 1E). Consequently, both groups exhibited less lean mass loss than did the OVX group (Fig. 1F). In agreement with these findings, MIS and 17β-E2 treatment resulted in an increased lean/fat mass ratio compared to that of their OVX counterparts from Day 30 onwards (Fig. 1G).

3.3. Effects of MIS and 17β-E2 interventions on cholesterol metabolism

Although no significant differences were observed in the circulating levels of TC and HDL-c among groups (Table 1), MIS resulted in a lower atherogenic TC/HDL-c ratio in the OVX-MIS group than in their OVX counterparts, and a similar result was found in the OVX-E2 group, although the differences were not statistically significant (Table 1). The OVX-E2 group exhibited significantly lower circulating levels of non-HDL-c than the OVX group (Table 1).

3.4. MIS and 17β-E2 treatments decreased risk factors for type 2 diabetes

In agreement with the decreased adiposity found in OVX-E2 rats and according to the well-known association between circulating levels of leptin and fat mass accretion, 17β-E2 treatment resulted in a significant decrease in plasma leptin levels, an effect that was nuanced in the OVX-MIS rats in which numerically lower values of this hormone were detected, although no significant differences were reported (Fig. 2E). OVX-E2 animals also displayed decreased circulating levels of adiponectin, whereas no significant differences were observed between OVX and OVX-MIS rats (Fig. 2F). No significant changes were found in plasma glucose levels among the groups (Table 1). Remarkably, 17β-E2 injections significantly counteracted the increases in the circulating levels of insulin (Fig. 2G) and in the surrogate marker of IR, HOMA-IR, observed in OVX rats (Fig. 2H) (28 % and 38 % lower, respectively, than those in the OVX group). MIS intake produced decreases in both parameters (22 % and 24 % lower for plasma insulin levels and HOMA-IR, respectively, than in the OVX group), although the differences were not statistically significant (Figs. 2G and 2H). Interestingly, both OVX-MIS and OVX-2 rats showed a significantly lower LAR -a suitable predictor of type 2 diabetes- than their OVX counterparts (Fig. 2I). A correlation analysis between HOMA-IR and the LAR revealed a strong positive correlation ($r = 0.585$, 95 % CI = 0.330–0.760, $p < 0.0005$). Notably, our analysis also revealed significant correlations between the area and number of adipocytes and these metabolic parameters. Thus, strong positive correlations were observed between the adipocyte area and HOMA-IR ($r = 0.672$, 95 % CI = 0.422–0.827, $p < 0.0005$) and between the adipocyte area and the LAR ($r = 0.734$, 95 % CI = 0.517–0.862, $p < 0.0005$). Conversely, strong inverse correlations were found between the number of adipocytes and the HOMA-IR score ($r = -0.583$, 95 % CI = −0.774 to −0.294, $p < 0.0005$) and between the number of adipocytes and the LAR ($r = -0.596$, 95 % CI = −0.782 to −0.312, $p < 0.0005$).

3.5. Effects of MIS and 17β-E2 injections on inflammatory and oxidative stress biomarkers

Concerning the levels of proinflammatory biomarkers analysed in plasma, no significant changes were observed in the circulating levels of the chemokine MCP-1 among the groups ($p= 0.238$, one-way ANOVA). Subsequent pairwise comparisons revealed that plasma MCP-1 concentrations tended to increase in OVX rats compared to those in their SHAM counterparts (34.1 % higher; $p=0.099$, Student's t test), and both the E2 and MIS treatments counteracted this increase, although the differences were not statistically significant with respect to their OVX counterparts (22.2 % and 18.5 % lower, $p=0.118$ and $p=0.102$, respectively, Student's t test) (Fig. 4A). In addition, an inverse correlation was observed between the adipocyte number and MCP1 levels ($r = -0.395$, 95 % CI = −0.653 to −0.053, $p < 0.0005$). Although the circulating levels of the acute proinflammatory marker CRP did not increase in OVX rats compared with SHAM rats, the animals that received the MIS displayed lower circulating levels of this protein than their OVX counterparts (Fig. 4B). Intriguingly, OVX-E2 rats showed a sharp increase (146 % higher compared with OVX animals) in the urinary levels of the marker of oxidative damage of DNA 8-OHdG [60] (Fig. 4C), an effect that was not observed in response to MIS treatment. Although no changes in total

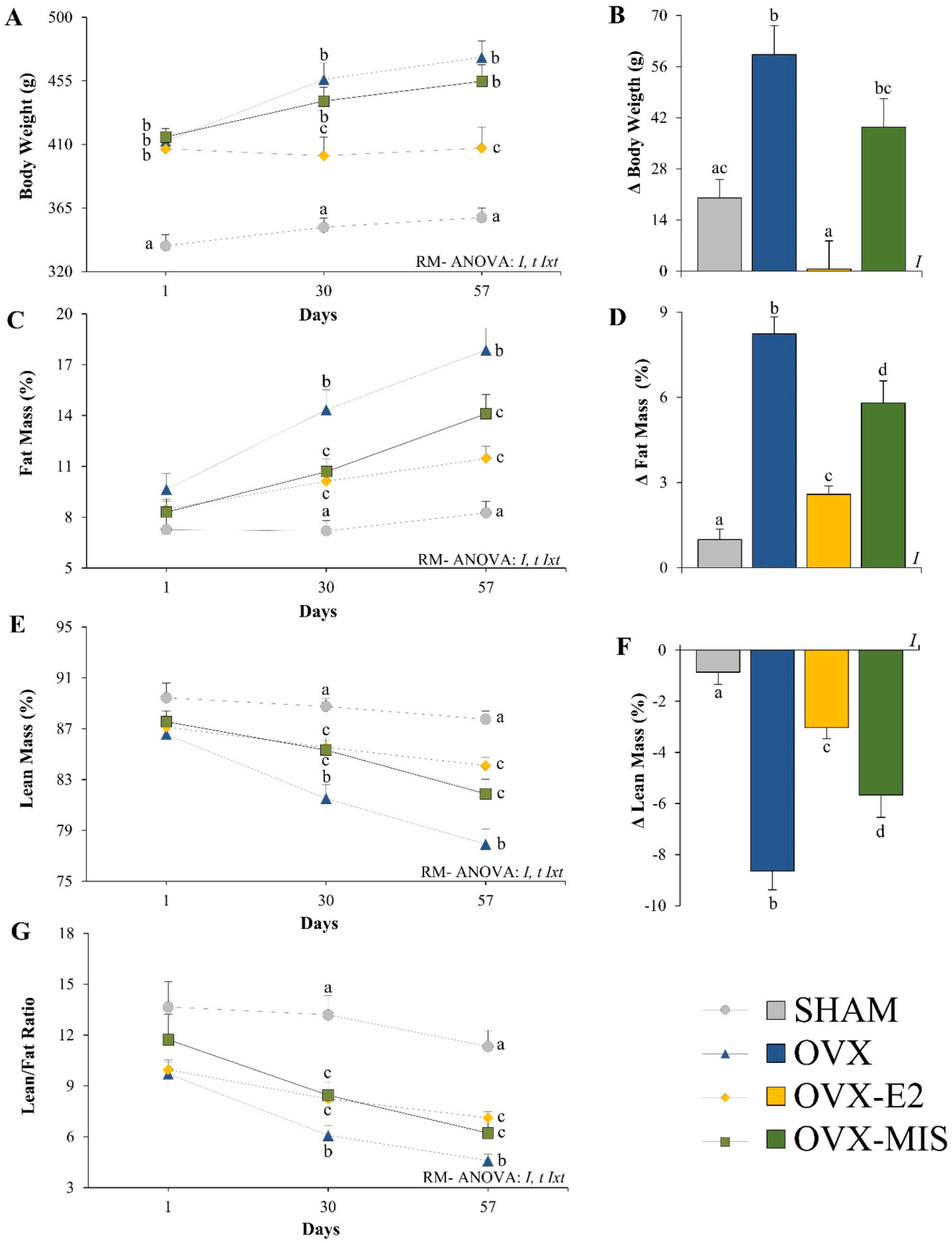

(caption on next page)

Fig. 1. Body weight (A), Δ body weight (B), fat mass (C), Δ fat mass (D), lean mass (E), Δ lean mass (F) and lean/fat ratio (G) in sham-operated (SHAM) and ovariectomized (OVX) rats after 8 weeks of intervention. The data are presented as the means ± SEMs (n = 10). Changes in body weight, fat mass and lean mass were calculated as the differences between the final and initial values of these parameters and are depicted in the Figs. 1B, 1D and 1F as Δ values. Figs. 1A, 1C, 1E and 1G: *I*: the effect of intervention, *t*: the effect of time, *Ixt*: the interaction between intervention and time (RM-ANOVA, $p<0.05$). When a significant interaction was observed between both factors, one-way ANOVA followed by Duncan's *post hoc* test or the Kruskal—Wallis test and Mann—Whitney U *post hoc* test ($p < 0.05$) were used to determine intervention-related differences at each time point among groups. Figs. 1B, 1D and 1F: *I*: the effect of the intervention (one-way ANOVA followed by Duncan's *post hoc* test or the Kruskal—Wallis test and Mann—Whitney U *post hoc* test; $p<0.05$). In all the figures, different superscript lowercase letters (a, b, c, d) indicate significantly different mean values among the groups. SHAM: sham-operated rats, OVX: ovariectomized rats, OVX-E2: OVX rats treated with 17β-oestradiol, OVX-MIS: OVX rats supplemented with the multi-ingredient.

GSH levels, reduced GSH levels or the GSH/GSSG ratio were detected among the groups (Figs. 4D, 4E & 4 G, respectively), all three OVX groups exhibited significantly higher hepatic levels of oxidized GSH than their SHAM counterparts, and any treatment could counteract this increase caused by ovariectomy (Fig. 4F).

3.6. 17β-E2 treatment improved BMC and biochemical markers of bone turnover

No significant changes in the weight or length of either femurs or tibias were found among the groups (Table 2). According to the μCT analyses performed on the right femur, no significant changes in BMD, BMC or TMC were observed among the groups (Table 2). However, 17β-E2 treatment resulted in an increased TMD in the femur, consistent with the effects of ovariectomy on the OVX group (Table 2). Moreover, μCT analyses of the right tibia revealed that 17β-E2 administration increased the BMC and TMC compared to those in the OVX group (Table 2). Concerning the circulating levels of the biomarkers of bone turnover, 17β-E2 injections counteracted the increase observed in the level of the biomarker of bone formation OC in the OVX animals and decreased the circulating levels of the bone resorption biomarker CTX-1, but the latter effect was not statistically significant (12.6 % lower, $p=0.188$ compared with OVX rats, Student's t test) (Table 2). Conversely, MIS consumption did not improve μCT-related parameters in either the femur or tibia and did not change the circulating levels of bone turnover biomarkers (Table 2).

3.7. Transcriptional changes in the RWAT of ovariectomized rats after MIS consumption

We performed a transcriptomic analysis of RWAT samples from OVX and OVX-MIS animals to provide insights into the mechanisms underlying the antiadiposity effects on OVX-MIS rats. KEGG pathway analysis of all the gene expression data revealed that the most significantly affected (downregulated) pathways encompassed a comprehensive range of immune, inflammation and defence processes, including the T-cell and B-cell receptor signalling pathways, cytokine—cytokine receptor interactions and chemokine signalling pathways, among others (Figure 5 A). Other frequently classified processes included cytoskeleton and cellular networks, such as focal adhesion and extracellular matrix (ECM) receptor interaction, as well as pathways related to the degradation of cellular components, such as the proteasome, endocytosis and lysosome (Figure 5 A). Furthermore, glycoconjugate and lipid metabolism, as well as pathways related to glucose homeostasis, were also affected (Figure 5 A). The DGE analysis revealed 188 genes that were differentially regulated between OVX and OVX-MIS animals, many of which (62.8 %, 118 genes) were downregulated (Figure 5B). Furthermore, hierarchical clustering analysis based on the significantly differentially expressed genes revealed distinct clustering patterns between the OVX and OVX-MIS groups (Figure 5 C). Of these 188 genes, 14 were unknown and therefore could not be grouped into any pathway. The 174 remaining known genes were distributed into different biological processes according to the information obtained via KEGG pathway analysis, enrichment analyses using the g:Profiler program, and information obtained from the scientific literature and various biological databases (NCBI, PubMed and Human Protein Atlas) (Figure 5D). The most representative biological processes were cell proliferation, differentiation and death, cytoskeleton and cellular network, and immunity, inflammation and response to stress (Figure 5D). Other biological processes that were also affected included energy homeostasis, carbohydrate and lipid metabolism, transport of small molecules (ions, amino acids and vitamins) and protein processing and ubiquitination (Figure 5D). The pathways related to these biological processes, as well as the most representative genes belonging to these pathways, are included in Table 3. The patterns of expression of many of these genes are analysed in the Discussion section.

3.8. MIS and 17β-E2 treatments did not increase EE or substrate oxidation

No significant variations were identified either in the RQ or in fat and carbohydrate oxidation among the groups (Supplementary Table 1). A lower EE was observed in both OVX and OVX-MIS animals than in their SHAM counterparts, after considering the whole 21-hour period and both the light and dark phases separately (Supplementary Table 1). A comparable pattern was observed in the animals that received the 17β-E2 injections, although the differences were not statistically significant compared to the SHAM animals across the entire 21-hour period and the dark phase (Supplementary Table 1).

3.9. MIS and 17β-E2 treatments did not affect anxiety-like behaviours or short-term memory

Rats were subjected to the EPM test to evaluate their anxiety-like behaviours and the effects of MIS and 17β-E2 treatments. No significant differences in any anxiety-like behaviour-related parameters were detected in the percentage of entries (in the open and enclosed arms, OAE % and EAE %, respectively) or in the time spent (in the central zone, open arm and enclosed arm, CT %, OAT % and EAT %, respectively) among the groups (Supplementary Figures 1 A and 1B). Animals were also challenged with the Y-maze to evaluate their short-term spatial reference memory and the effects of MIS and 17β-E2 treatments. No differences were detected among the experimental groups in terms of the percentage of entries and time spent in the novel arm (novel arm preference index (%)) or spontaneous alternation (%) (Supplementary Figures 1C-E).

4. Discussion

In this study, we examined the effects of the intake of the MIS containing histidine, carnosine, cysteine and serine for 8 weeks on menopause-related complications in OVX rats, a well-established preclinical model of postmenopausal oestrogen deficiency. We described that OVX rats exhibit different hallmarks that can appear in the postmenopausal state, such as body weight gain, fat mass accretion, adipocyte hypertrophy, IR and greater risks of CVD and osteoporosis, as was previously reported [61,62]. Remarkably, MIS consumption exerted beneficial effects on many of the aforementioned alterations, including (1) decreased adiposity and RWAT adipocyte hypertrophy, (2) improved body composition, as evidenced by the increased lean body mass and lean/fat mass ratio, (3) reduced LAR and TC/HDL-c ratio, (4) decreased circulating levels of the proinflammatory marker CRP, and (5) improved

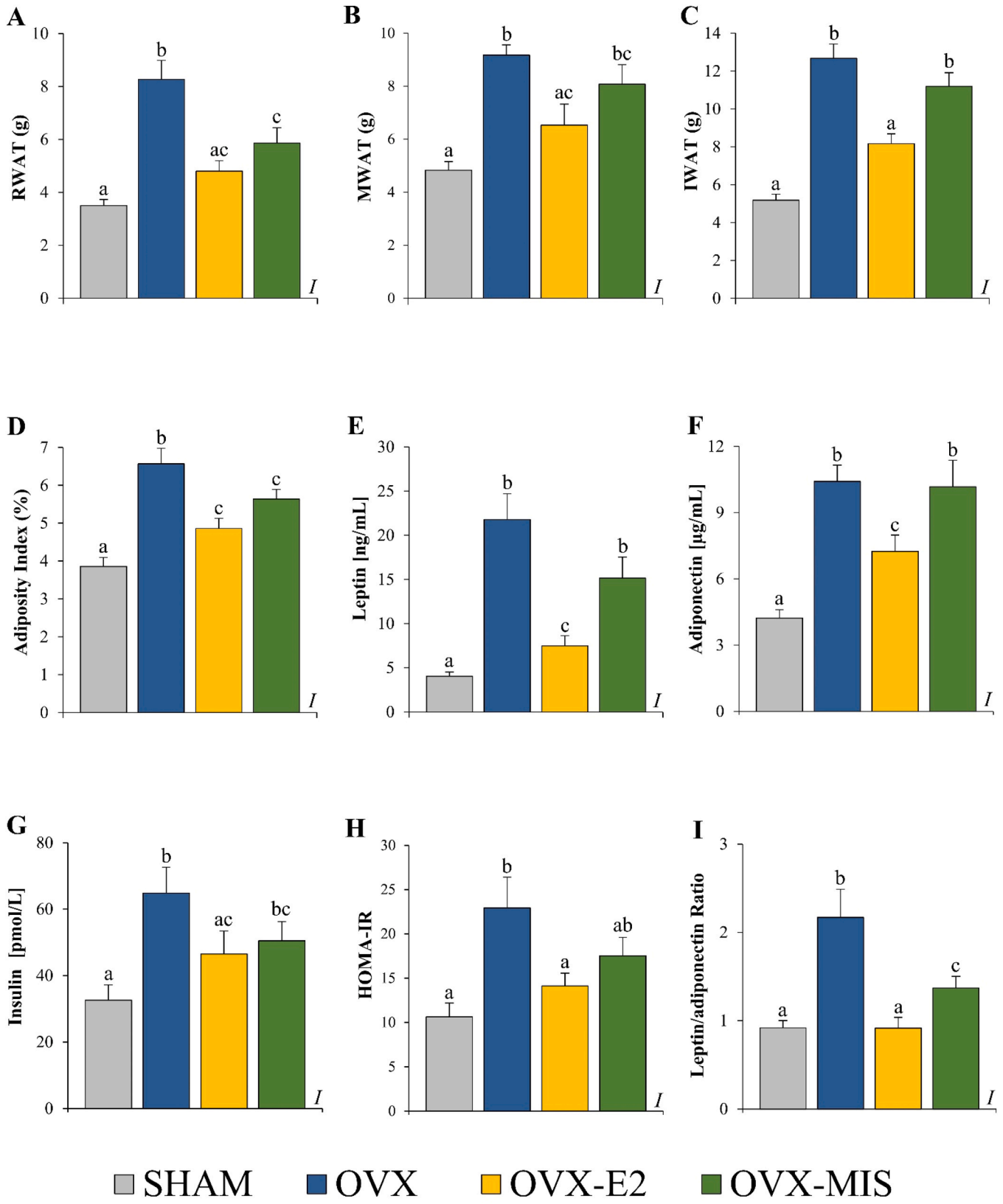

Fig. 2. Effects of ovariectomy, 17β-E2 injections and MIS treatment on MWAT (A), RWAT (B), and IWAT (C) depot weights; the adiposity index (D); the circulating levels of leptin (E), adiponectin (F) and insulin (G); HOMA-IR (H); and the leptin/adiponectin ratio (I) in sham-operated (SHAM) and ovariectomized (OVX) rats after 8 weeks of intervention. The data are presented as the means ± SEMs (n = 9–10). In each figure, different superscript lowercase letters (a, b, c) indicate significantly different mean values among groups (one-way ANOVA and Duncan's *post hoc* test, $p < 0.05$). *I:* effect of the intervention. SHAM: sham-operated rats, OVX: ovariectomized rats, OVX-E2: OVX rats treated with 17β-oestradiol, OVX-MIS: OVX rats supplemented with the multi-ingredient. HOMA-IR: homeostasis model assessment-estimated insulin resistance; IWAT: inguinal white adipose tissue; MWAT: mesenteric white adipose tissue; RWAT: retroperitoneal white adipose tissue.

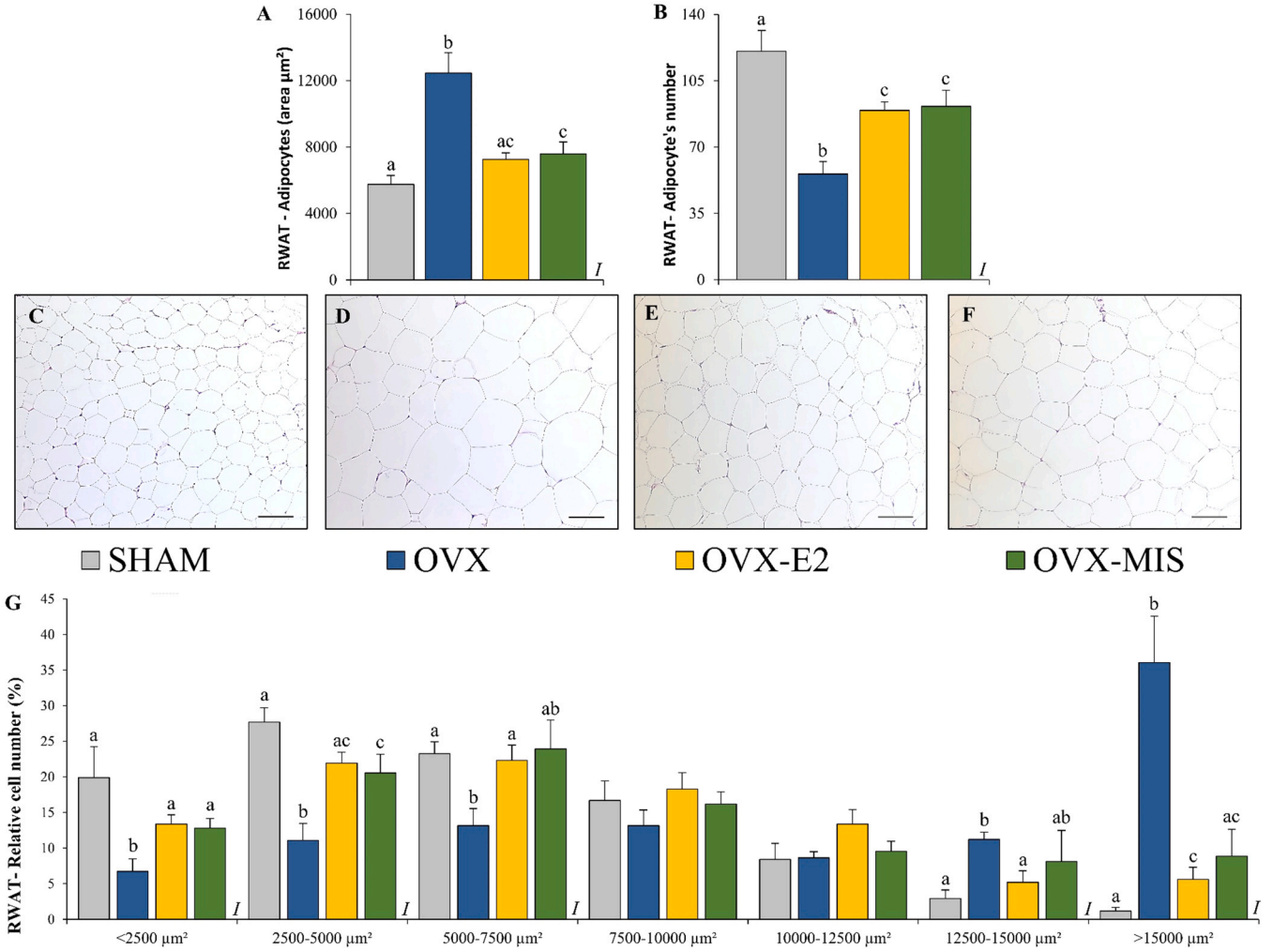

Fig. 3. Effects of ovariectomy, 17β-E2 injections and MIS treatment on the adipocyte area (A) and number of adipocytes (B); representative micrographs of haematoxylin–eosin-stained RWAT sections (bar = 100 µm) (C-F, respectively) and adipocyte size distribution (G) of the SHAM, OVX, OVX-E2 and OVX-MIS groups after 8 weeks of intervention. The data are presented as the means ± SEM (n = 8). In each figure, different superscript lowercase letters (a, b, c) indicate significantly different mean values among groups (one-way ANOVA and Duncan's *post hoc* test or Kruskal—Wallis test and Mann—Whitney U *post hoc* test, $p < 0.05$). *I:* effect of the intervention. SHAM: sham-operated rats, OVX: ovariectomized rats, OVX-E2: OVX rats treated with 17β-oestradiol, OVX-MIS: OVX rats supplemented with the multi-ingredient. RWAT: retroperitoneal white adipose tissue.

RWAT gene expression profile towards better adipocyte structure, morphology and immunometabolic function. Overall, these findings confirmed our hypothesis and highlighted the potential of the consumption of this amino acid-related MIS as an alternative therapy for managing obesity and improving immunometabolic health in menopausal women.

The reduced adiposity observed in OVX rats that received the MIS compared to their OVX counterparts shown herein could be attributed, at first glance, to the protective effect on obesity that has been previously reported for different amino acids, including histidine and carnosine, and, to a much lesser extent, for serine and cysteine, in both animal models and humans [21,27,28]. Nevertheless, to the best of our knowledge, very limited data are available regarding the antiobesity effects of these four bioactive compounds administered alone or in combination on OVX rodent models. To the best of our knowledge, only one study has focused on the effects of a 5-day treatment with histidine between non-ovariectomized and OVX rats in the context of obesity, reporting a lower suppressive effect on food intake in OVX animals than in their counterparts and suggesting the activation of histamine neurons as a possible potential mechanism to explain the described effects [63]. The decreased EE reported in OVX rats compared to their SHAM counterparts was consistent with numerous studies showing that the body weight gain accompanied by progressive fat accretion occurring in menopausal and postmenopausal women can be associated with a decreased EE [64,65]. In the present study, a reasonable speculation was that the intake of the MIS could mitigate fat mass gain through the enhancement of EE and the inhibition of food intake, two well-established mechanisms by which different bioactive compounds could exert their beneficial effects [65]. In this context, two studies showed that the intake of histidine decreased food intake, which was accompanied by decreased RWAT weight in aged male Wistar rats [66,67]. Furthermore, López-Gonzales et al. showed that serine supplementation increased EE by activating brown fat thermogenesis in high-fat diet-fed C57BL/6 N-Rj male mice [68], and long-term L-serine administration for 6 months to aged C57BL/6 J mice significantly reduced food intake and body weight gain [24]. In our study, the lack of effects on food intake and EE observed in OVX-MIS *versus* OVX rats indicated that the modulation of these processes was not the mechanism underlying the antiobesity effects observed in response to MIS consumption.

Two additional mechanisms involved in the effects of bioactive compounds against fat accretion are the activation of lipid catabolism-related pathways (lipolysis and β-oxidation) and the inhibition of lipogenesis. At first glance, the increased mRNA levels of the gene encoding

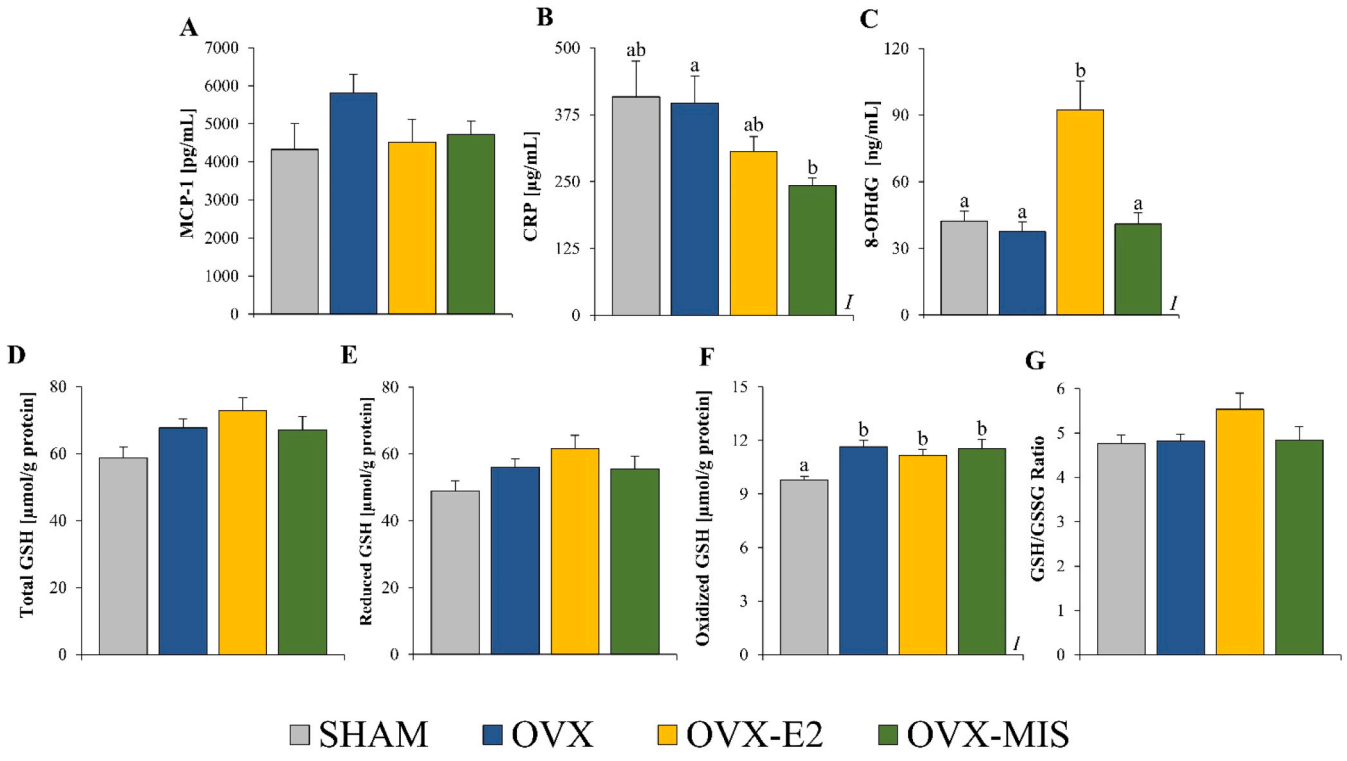

Fig. 4. Effects of ovariectomy, 17β-E2 injections and MIS treatment on the circulating levels of MCP-1 (A) and CRP (B); urinary 8-OHdG concentrations (C); total GSH (D), reduced GSH (E) and oxidized GSH levels in the liver (F); and the hepatic GSH/GSSG ratio (G) in sham-operated (SHAM) and ovariectomized (OVX) rats after 8 weeks of intervention. The data are presented as the means ± SEMs (n = 9–10). In the figures, different superscript lowercase letters (a, b) indicate significantly different mean values among groups (one-way ANOVA and Duncan's *post hoc* test or Kruskal—Wallis test and Mann—Whitney U *post hoc* test, $p < 0.05$). *I:* effect of the intervention. SHAM: sham-operated rats, OVX: ovariectomized rats, OVX-E2: OVX rats treated with 17β-oestradiol, OVX-MIS: OVX rats supplemented with the multi-ingredient. MCP-1: monocyte chemoattractant protein-1; CRP: C-reactive protein; 8-OHdG: 8-hydroxy-2′-deoxyguanosine; GSH: glutathione; GSSG: oxidized glutathione.

peroxisomal ACOT4 observed in the RWAT of OVX-MI animals could suggest the activation of β-oxidation, since the acyl-CoA esters are transported into the peroxisome via ABCD transporters and undergo β-oxidation, and the resulting products succinyl-CoA and glutaryl-CoA can be hydrolysed by this auxiliary enzyme to obtain succinate and glutarate, which are subsequently transported to mitochondria [69]. Nevertheless, we did not observe changes in the mRNA levels of key genes involved in lipolysis (*Hsl* and *Atgl*), β-oxidation (*Cpt1b* and *Had*) or lipogenesis (*Acc1*, *Fas, Gpat*, and *Dgat2*); therefore, the reported anti-obesity effect of MIS is not due to the modulation of these key lipid-related pathways in the RWAT, at least at the gene expression level.

The beneficial effect on fat mass accretion reported in the OVX-MIS animals, although significant, was weaker than we observed in response to 17β-E2 injections. This superior effect observed on OVX-E2 animals could be attributed to their decreased food intake, one effect that was previously described [70] and that also contributed to explaining the clear decrease in body weight and body weight gain observed in response to this pharmacological treatment, which was not significantly reported after MIS consumption. Remarkably, both groups of treated rats displayed a lower loss of lean mass than their OVX counterparts over time, which is indicative of greater muscle mass accretion [71] and explains, at least in part, why the decreased adiposity reported after MIS consumption was not accompanied by significantly lower body weight in OVX-MIS rats. The increased lean/fat mass ratio found in both OVX-MIS and OVX-E2 animals reinforces the idea that both 17β-E2 injections and MIS consumption promoted a shift towards a healthier body composition in OVX rats [72], which was previously described by our group in response to other bioactive compounds [14].

The hypertrophy observed in the RWAT of OVX animals compared to that in their SHAM counterparts, which was accompanied by increased circulating levels of insulin, HOMA-IR and LAR, a reliable biomarker of MetS and diabetes risk, is consistent with scientific evidence indicating that WAT hypertrophy is associated with IR and inflammation [73]. Thus, the lower RWAT hypertrophy observed in both OVX-E2 and OVX-MIS animals compared to OVX rats could explain, at least in part, the improved metabolic health observed in both groups of animals, as evidenced by the decreases in the LAR, the circulating levels of insulin and the HOMA-IR, although the differences in these two latter parameters were statistically significant only for the rats that received the E2 injections. Although correlations do not imply causality, the strong positive correlations found between HOMA-IR/LAR and the adipocyte area of the RWAT in all the animals included in the study, as well as the decreased circulating CRP levels reported in OVX-MIS rats, also suggest an improvement in the immunometabolic health of the rats that received the MIS.

Our RWAT transcriptomic analysis reinforced our hypothesis that decreased hypertrophy in response to MIS consumption is associated with an immunometabolic benefit. Thus, the increased mRNA levels of the gene encoding ZFP407, which stimulates insulin-mediated glucose uptake in adipocytes and protects against adipocyte hypertrophy and IR in mice [74], as well as the overexpression of the gene encoding GABRG3, a γ-aminobutyric acid (GABA) receptor that mediates the antiadipogenic, antidiabetic and anti-inflammatory effects of GABA [75, 76], which is found in the RWAT of OVX-MIS animals, are consistent with this idea. We also detected marked overexpression of *Gcgr*, a gene that encodes the glucagon receptor, which is expressed (at low levels) in WAT and mediates both lipolysis and glucose uptake induced by glucagon in adipocytes. Remarkably, in humans, *GCGR* expression was positively associated with a reduction in both the visceral and subcutaneous WAT volume and with improved insulin sensitivity, and in

Table 2
Bone-related parameters in sham-operated (SH) and ovariectomized (OVX) rats after 8 weeks of intervention.

	SHAM	OVX	OVX-E2	OVX-MIS	Intervention effect
Biometric parameters					
Femurs (g)	2.26 ± 0.04	2.38 ± 0.06	2.28 ± 0.05	2.31 ± 0.04	NS (0.350)
Femurs (cm)	3.80 ± 0.03	3.88 ± 0.03	3.83 ± 0.03	3.91 ± 0.03	NS 0.058)
Tibias (g)	1.82 ± 0.03	1.93 ± 0.05	1.89 ± 0.04	1.91 ± 0.04	NS (0.282)
Tibias (cm)	1.21 ± 0.04	0.93 ± 0.04	1.09 ± 0.02	0.97 ± 0.02	NS (0.304)
Microcomputed tomography analyses (μCT)					
Right femur (μCT)					
BMD (mg/cc)	356 ± 14	328 ± 14	343 ± 9	312 ± 10	NS (0.074)
TMD (mg/cc)	1020 ± 14^{a}	936 ± 10^{b}	977 ± 19^{c}	920 ± 12^{b}	*I* (<0.001)
BMC (mg)	142 ± 6	140 ± 3	145 ± 4	138 ± 3	NS (0.717)
TMC (mg)	137 ± 6	135 ± 3	139 ± 4	132 ± 2	NS (0.790)
Right tibia (μCT)					
BMD (mg/cc)	271 ± 15^{a}	224 ± 8^{b}	228 ± 11^{b}	201 ± 7^{b}	*I* (0.003)
TMD (mg/cc)	900 ± 24^{a}	793 ± 9^{bc}	838 ± 21^{b}	779 ± 11^{c}	*I* (<0.001)
BMC (mg)	140 ± 5^{ab}	134 ± 3^{b}	153 ± 7^{a}	134 ± 4^{b}	*I* (<0.001)
TMC (mg)	135 ± 5^{ab}	128 ± 2^{b}	147 ± 6^{a}	127 ± 4^{b}	*I* (0.015)
Plasma parameters					
OC (ng/mL)	114 ± 10^{a}	209 ± 24^{b}	137 ± 4^{a}	245 ± 14^{b}	*I* (<0.001)
CTX−1 (ng/mL)	14.4 ± 1.3^{a}	22.0 ± 1.1^{bc}	19.2 ± 1.7^{b}	23.5 ± 1.5^{c}	*I* (<0.001)
PINP (ng/mL)	7.94 ± 0.66	11.10 ± 1.51	8.22 ± 0.36	8.29 ± 0.50	NS (0.463)

Data are presented as the means ± SEMs (n = 9–10). Different superscript lowercase letters (a, b, c) indicate significantly different mean values (one-way ANOVA and Duncan's *post hoc* test, $p < 0.05$). *I*: effect of the intervention. NS: nonsignificant differences. SHAM: sham-operated rats; OVX: ovariectomized rats; OVX-E2: OVX rats treated with 17β-oestradiol; OVX-MIS: OVX rats supplemented with the multi-ingredient; OC: osteocalcin; CTX-1: carboxy-terminal telopeptide of type I collagen; PINP: procollagen I amino-terminal propeptide; BMD: bone mineral density; TMD: tissue mineral density; BMC: bone mineral content; TMC: tissue mineral content.

rodents, GCGR activation protected against obesity [77,78]. The decreased expression of *Grb14*, a negative regulator of the insulin receptor signalling pathway that is overexpressed in the WAT of obese animals and humans and/or in individuals with type 2 diabetes [79–81], in the RWAT of OVX-MIS animals supports our hypothesis.

Obesity is characterized by increased collagen production in WAT, which can be interpreted as an adaptative response to fat mass accretion, requiring the remodelling of the ECM to support adipocyte growth [82–84]. The downregulation of a plethora of genes involved in cytoskeletal organization (*Actb*, *Lcp1* and *Pfn1*), cell adhesion (*Fermt3* and *Cdh11*) and ECM remodelling, such as those related to collagen metabolism (*Col1a2*, *Col5a1*, *Col5a2*, *Creb3l1*, *Bmp2*, *Sparc*, *Bgn*, *Lox* and *Serpinh1*) and proteolytic degradation of ECM (*Timp1* and *Htra1*) observed in the RWAT of OVX-MIS animals is consistent with the protective effect on adipocyte hypertrophy observed in response to the consumption of this blend of amino acid-related compounds. Interestingly, most of these genes that were downregulated in our study have been shown to be upregulated with obesity and positively correlated with markers of IR and inflammation. Thus, CREB3L1 is a transcription factor that can be activated by BMP2, which induces the expression of *Col1a1*, *Col5a1* and possibly *Col1a2* [85], the levels of which were increased in the epididymal WAT of obese and type II diabetic *db/db* mice [82]. LOX is a protein that boosts collagen crosslinking in the ECM and enhances adipocyte tissue stiffness, and its activity and mRNA and protein levels are increased in adipocytes and adipose tissue macrophages (ATMs) of both mice and humans with obesity [86,87]. The levels of the tissue inhibitor of matrix metalloproteinase 1 (TIMP1), which suppresses the transformation of the ECM, were increased in the WAT [88,89] of obese mice. In addition, *Timp1* mRNA levels are positively correlated with gonadal fat weight [89]. Similarly, the expression of the gene encoding SPARC, an ECM-related protein involved in adipose tissue remodelling and fibrosis due to its role in collagen assembly, was increased in animal models and humans with obesity [90–92], and SPARC mRNA and/or circulating protein levels were positively correlated with BMI, fasting insulin levels, HOMA-IR and CRP in humans [90–92] and with waist circumference and total adipose tissue area in women [92]. Furthermore, the mRNA levels of the gene encoding biglycan (BGN), which interacts with collagens and elastins in the ECM, were higher in both subcutaneous and visceral adipose tissues from obese women than in those from normal-weight women and were positively correlated with BMI, adipocyte size and total adipose tissue area [93]. In addition, biglycan mRNA levels are positively correlated with the circulating levels of CRP, insulin, HOMA-IR and leptin in women [93]. The decreased mRNA levels of *Serpinh1*, which encodes the collagen-specific molecular chaperone HSP47 observed in the RWAT of OVX-MIS animals are also consistent with the idea that MIS intake led to a favourable adaptative response to the adipocyte hypertrophy. Thus, *HSP47* expression increases with obesity and in response to insulin and is positively correlated with BMI, fat mass, and waist and hip circumferences in humans [94]. Altogether, these results strongly suggest that the decreased RWAT weight and hypertrophy observed in OVX-MIS animals was reflected at gene expression level in improvements in the structure, morphology and immunometabolic function of their adipocytes.

The sharp downregulation of the mRNA levels of genes mainly expressed in hypertrophied WAT by ATMs and encoding proteins involved in cytokine (IL1B, FASLG, and PTGS2)- and chemokine (CXCL2, CCR7)-mediated inflammation, whose levels were increased in WAT in the obese state [95–99] and correlated with macrophage infiltration and adipocyte size in visceral WAT [96], strongly suggested that MIS consumption ameliorated the low-grade inflammation in WAT that occurred as a consequence of the fat accretion produced in OVX rats after ovariectomy. The decreased *Cd5l* and *Btk* expression levels found in the RWAT of OVX-MIS animals reinforce this idea. Notably, *Cd5l* encodes the apoptosis inhibitor of macrophages (AIM)/CD5L, which plays an important role in the crosstalk between adipocytes and macrophages, activating the TLR-4 pathway in individuals with obesity and, therefore, triggering the secretion of proinflammatory chemokines, such as MCP-1, to induce the recruitment of proinflammatory M1 macrophages to WAT [100]. The downregulation of the gene encoding BTK, a kinase that enhances the proinflammatory response in macrophages through NF-κB and NLRP3 inflammasome activity and is overexpressed in diet-induced obese mice [101] and patients with obesity and diabetes [102], provides additional scientific evidence supporting our hypothesis. Thus, the inhibition of BKT signalling promoted an anti-inflammatory M2-like phenotype in macrophages through the activation of oxidative phosphorylation (OxPhos) via the upregulation of different genes related to the mitochondrial electron transport chain, including *Mt-co2* [102], which was also overexpressed in the present study. The significantly increased expression of three additional genes related to mitochondrial respiratory chain complex I (*Mt-nd5*, *Mt-nd6* and *Nubpl*) found in OVX-MIS animals suggests, at first glance, an immune-related benefit of the MIS in RWAT by enhancing the M2-like phenotype in macrophages through the activation of OxPhos, although additional research is needed to shed more light on this issue.

At first glance, the lower mRNA levels of the genes involved in the

Table 3
Functional categorization of differentially expressed genes in the RWAT of OVX-MIS rats.

Biological process	*Main-related pathway*	*Gene name*	*Gene symbol*	*Gene ID*	*FC*	*Adj. p value*
Immunity, inflammation and response to stress	Cytokine mediated inflammation	*Interleukin 1 beta*	*Il1b*	24494	−2.11	0.095
		Fas ligand	*Faslg*	25385	−1.63	0.077
		Prostaglandin-endoperoxide synthase 2	*Ptgs2*	25526	−1.90	0.087
	Chemokine mediated inflammation	*C-X-C motif chemokine ligand 2*	*Cxcl2*	114105	−7.19	0.022
		C-C motif chemokine receptor 7	*Ccr7*	287673	−2.97	0.001
	Immune cell-cell communication	*Cd5 molecule-like*	*Cd5l*	310693	−3.95	0.099
		Cd28 molecule	*Cd28*	25660	−1.67	0.030
		C-type lectin domain family 4, member A2	*Clec4a2*	297584	−3.56	0.000
	Signalling	*Fc gamma receptor 1 A*	*Fcgr1a*	295279	−1.58	0.032
		Spi-B transcription factor	*Spib*	499146	−2.84	0.032
		Bruton tyrosine kinase	*Btk*	367901	−1.46	0.093
Lipid metabolism	Fatty acid metabolism	*Fatty acid binding protein 3*	*Fabp3*	79131	−2.20	0.086
		Acyl-coa thioesterase 4	*Acot4*	681337	1.56	0.088
	Sterol metabolism	*Cytochrome P450, family 11, subfamily a, polypeptide 1*	*Cyp11a1*	29680	−1.65	0.053
		Oxidized low density lipoprotein receptor 1	*Olr1*	140914	−3.35	0.030
		Vacuole membrane protein 1	*Vmp1*	192129	−1.30	0.059
	Phospholipid metabolism	*Sphingomyelin synthase 2*	*Sgms2*	310849	−1.58	0.002
		Sphingomyelin phosphodiesterase 3	*Smpd3*	94338	−1.68	0.041
Carbohydrate metabolism	Glucose and insulin homeostasis	*Growth factor receptor bound protein 14*	*Grb14*	58844	−1.51	0.030
		Gamma-aminobutyric acid type A receptor subunit gamma 3	*Gabrg3*	79211	1.82	0.084
		Zinc finger protein 407	*Zfp407*	307213	1.23	0.010
		Glucagon receptor	*Gcgr*	24953	2.82	0.022
Cell proliferation, differentiation and death	Cell fate determination and differentiation	Fosb proto-oncogene, AP−1 transcription factor subunit	*Fosb*	100360880	−2.78	0.000
		Fos proto-oncogene, AP−1 transcription factor subunit	*Fos*	314322	−2.46	0.032
		Cellular communication network factor 5	*Ccn5*	29576	−4.51	0.032
		Mesenteric oestrogen-dependent adipogenesis	*Medag*	360757	−1.40	0.062
		GLI pathogenesis-related 1	*Glipr1*	299783	−1.62	0.030
		Growth differentiation factor 10	*Gdf10*	79216	−1.83	0.099
		Activating transcription factor 5	*Atf5*	282840	−1.46	0.023
		Secreted frizzled-related protein 2	*Sfrp2*	310552	−1.63	0.010
		Bone morphogenetic protein 2	*Bmp2*	29373	−1.30	0.019
		Snail family transcriptional repressor 1	*Snai1*	1164903	−1.43	0.100
		Early growth response 2	*Egr2*	114090	−1.91	0.068
		V-set immunoregulatory receptor	*Vsir*	690899	−1.30	0.068
		Tax1 binding protein 3	*Tax1bp3*	360564	−1.28	0.088
		Activating transcription factor 3	*Atf3*	25389	−1.51	0.092
		Early growth response 1	*Egr1*	24330	−1.50	0.037
	Cell proliferation	Marker of proliferation Ki−67	*Mki67*	291234	−1.46	0.030
	Cell death - *Apoptosis*	*Niban apoptosis regulator 2*	*Niban2*	362115	−1.19	0.061
		BCL2-related protein A1	*Bcl2a1*	170929	−1.73	0.055
Cytoskeleton and cellular network	Extracellular matrix organization	*Thrombospondin 2*	*Thbs2*	292406	−1.69	0.032
		Secreted protein acidic and cysteine rich	*Sparc*	24791	−1.32	0.041
		Lysyl oxidase	*Lox*	24914	−1.63	0.011
		Htra serine peptidase 1	*Htra1*	65164	−1.15	0.063
		Camp responsive element binding protein 3-like 1	*Creb3l1*	362165	−1.35	0.087
		Biglycan	*Bgn*	25181	−1.51	0.084
		TIMP metallopeptidase inhibitor 1	*Timp1*	116510	−2.40	0.012
		Collagen type I alpha 2 chain	*Col1a2*	84352	−1.47	0.096
		Collagen type V alpha 1 chain	*Col5a1*	85490	−1.23	0.066
		Collagen type V alpha 2 chain	*Col5a2*	85250	−1.21	0.041
		Serpinh1 serpin family H member 1	*Serpinh1*	29345	−1.32	0.002
	Regulation of actin cytoskeleton	*Lymphocyte cytosolic protein 1*	*Lcp1*	306071	−1.52	0.092
		Profilin 1	*Pfn1*	64303	−1.25	0.068
	Cell adhesion	*FERM domain containing kindlin 3*	*Fermt3*	309186	−1.52	0.099
		Cadherin 11	*Cdh11*	84407	−1.87	0.065
	Cytoskeletal filaments	*Actin, beta*	*Actb*	81822	−1.23	0.048
Energy homeostasis	Mitochondrial ATP system/oxidative phosphorylation	*Uncoupling protein 2*	*Ucp2*	54315	−1.24	0.054
		Cytochrome c oxidase II, mitochondrial	*Mt-co2*	26198	1.44	0.022
		NADH dehydrogenase 5, mitochondrial	*Mt-nd5*	26202	1.40	0.075
		NADH dehydrogenase 6, mitochondrial	*Mt-nd6*	26203	1.43	0.013
		NUBP iron-sulfur cluster assembly factor like	*Nubpl*	299008	1.37	0.061
	Cellular energy sensing	*Nicotinamide nucleotide adenylyltransferase 2*	*Nmnat2*	289095	1.66	0.030

Abbreviations: RWAT, retroperitoneal white adipose tissue; FDR, false discovery rate; MIS, multi-ingredient supplementation; OVX, ovariectomized rats. FC: fold changes in OVX-MIS vs. OVX animals. The + symbol indicates upregulation, and the - symbol indicates downregulation in the OVX-MIS animals. Genes with FDR-derived *adj. p* value < 0.1 from the microarray data analysis are shown.

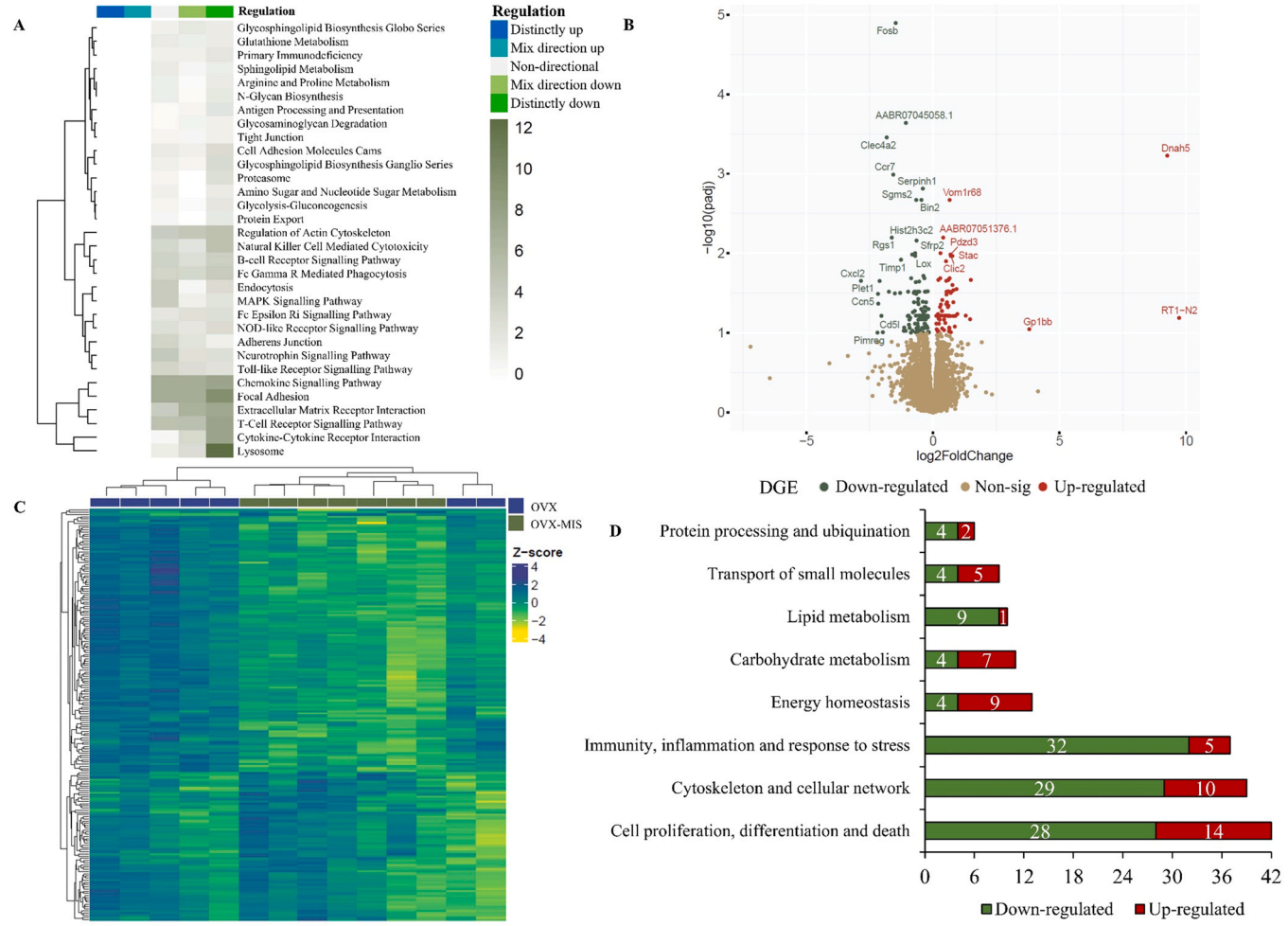

Fig. 5. Transcriptional changes in the RWAT of OVX and OVX-MIS rats (n =7 per group) after 8 weeks of intervention. Fig. 5A, Heatmap visualizing significantly regulated KEGG pathways (*adj.* $p < 0.05$) in the OVX-MIS group compared with the OVX group. The colour scale represents negative log10 scale adjusted p values of classes with different directions of regulation. Fig. 5B, Volcano plot visualizing changes in gene expression in the RWAT of OVX-MIS rats compared with OVX animals. Significantly downregulated and upregulated genes are highlighted with an *adj.* $p < 0.1$ and a log2(fold change) ≤ -1 or ≥ 1 and are shown in green and red, respectively. Fig. 5C, Heatmap visualizing the expression pattern of the 188 significant genes with an *adj.* $p < 0.1$ represented by Z score-transformed log2 counts per million. The column annotation represents the OVX and OVX-MIS intervention groups. Fig. 5D, Classification of the biological processes of the 188 genes that were differentially expressed (adj. $p < 0.1$) between the OVX-MI and OVX animals. OVX: ovariectomized rats; OVX-MIS: ovariectomized rats supplemented with the multi-ingredient; KEGG: Kyoto Encyclopedia of Genes and Genomes; RWAT: retroperitoneal white adipose tissue.

negative regulation of adipogenesis through the Wnt signalling pathway *Sparc* [103], *Timp1* [104] and *Ccn5* [105] as well as the decreased expression of the gene encoding the ECM-related protein TSP2 (also known as THBS2), which has been shown to have an inhibitory effect on adipogenesis [106], could suggest that MIS would activate adipogenesis in the RWAT of OVX-MIS rats through the downregulation of these genes. The observed downregulation of the genes encoding the transcription factors ATF3 [107] and EGR1 [108] and the proteins SNAIL1 [109] and GDF10, also known as BMP3B [110], which inhibit adipocyte differentiation, would also be, at first glance, consistent with an enhancement of the adipogenic program in the RWAT in response to MIS intake. These results are reinforced by the increased number of adipocytes found in the RWAT of both OVX-E2 and OVX-MIS animals compared to OVX rats according to histological analyses, and the strong inverse correlation pattern observed between the adipocyte number and HOMA-IR/LAR is in agreement with the idea that adipocyte hyperplasia protects against metabolic dysfunctions and preserves adequate WAT expansion [73]. Conversely, our findings also revealed decreased mRNA levels of genes encoding important transcription factors (FOS [111], FOSB [111], ATF5 [112], and EGR2 [108]) and proteins (MEDAG [113], GLIPR1 [114], SFRP2 [115], BMP2 [116] and VSIR [117]) involved in the activation of adipogenesis, which would not support the increased formation of adipocytes. Remarkably, we did not observe significant increases in the expression of the adipogenesis gatekeeper preadipocyte factor 1 [118] (*Pref-1*, also known as *Dk1,* which was sharply decreased in our study, FC: −11.7; p adj.=0.21) or in the mRNA levels of the genes encoding the master regulators of adipogenesis, PPARγ and C/EBPα [73, 118]. Overall, our findings did not support increased adipogenesis in the RWAT of OVX-MIS animals, although additional research focused on the protein levels of key factors involved in the adipogenic program and/or on the quantification of RWAT DNA content would be useful for shedding more light on this issue. Notably, many of the genes involved in cell fate determination and differentiation that were downregulated in the RWAT of OVX-MIS rats are increased with obesity (e.g., *Egr1* [119], *Egr2* [120], *Ccn5* [105], *Medag* [113], *Gdf10* [110], *Atf 3* [121], *Atf5* [112], *Sfrp2* [115], and *Bmp2* [116]), and some of these genes are involved in obesity-related metabolic alterations, such as IR/type 2 diabetes (*Egr1* [119], *Ccn5* [105], *Atf3* [121], *Sfrp2* [115], and *Bmp2* [116]), low-grade chronic inflammation (*Egr1* [119], *Egr2* [120], and *Fos* [122]) and the cellular stress response (*Egr1*, *Egr2, Fos*, *Fosb* and *Atf3*) [123]. Interestingly, fat or weight loss was associated with the downregulation of *FOS* [124] and *SFRP2* [125] expression in human WAT. Overall, these results

indicate that the modulation of these genes, which play important roles in adipose tissue function and stress response, is a favourable adaptive response to the decreased fat accretion and hypertrophy observed in the RWAT of OVX-MIS rats, which reinforces our hypothesis that an improved immunometabolic profile occurs in response to MIS consumption.

Supplementation with MIS also produced slight beneficial effects on cholesterol metabolism, significantly decreasing the TC/HDL-c ratio compared to that in their OVX counterparts. This atherogenic ratio, called the Castelli risk index 1 [126], constitutes a risk indicator for CVD with greater predictive value than each variable separately since an increase in the TC concentration is a marker of atherogenic lipoproteins, while a decrease in the HDL-C concentration is correlated with numerous risk factors, including the components of MetS. At first glance, this result could be partly attributed to the antihypercholesterolaemic and antiatherosclerotic effects of carnosine, which can facilitate the removal of aldehydes from atherosclerotic lesions [127] and counteract the increased circulating levels of TC and LDL-c in rats fed a high-fat high-carbohydrate diet [128]. Nevertheless, in the present study, OVX rats did not show significant changes in either TC levels or the TC/HDL-c ratio compared to SHAM animals. Therefore, additional studies in which OVX rats are challenged with a hyperlipidic and atherogenic diet to induce hypercholesterolemia would be valuable to provide more insights into the physiological significance of this effect. These slight positive effects observed regarding cholesterol homeostasis after MIS consumption were also observed at gene expression level in the RWAT of OVX-MI animals with the sharp downregulation of the gene encoding OLR1 (also named LOX-1), which is a receptor for oxidized LDL that enhanced the expression of proinflammatory cytokines in WAT and that was increased in diet-induced obese mice [129]. Furthermore, increased circulating LOX-1 levels were found in menopausal women with obesity, and the plasma levels of this protein positively correlated with BMI and body fat [130], suggesting that the downregulation of *Olr1* observed in the present study would also favour a healthier immunometabolic profile in the RWAT of OVX-MIS rats.

Surprisingly, we did not observe increased hepatic GSH levels in response to MIS consumption, contrary to what would be expected in response to the consumption of the potent GSH precursors serine and cysteine, which, in combination with L-carnitine and nicotinamide riboside, have been proposed as treatments for NAFLD in humans [131]. Remarkably, the increased urinary levels of 8-OHdG observed in OVX-E2 animals, an effect that was not observed after MIS consumption, could be interpreted as a side effect of the 7β-E2 treatment because the 8-OHdG levels increased in response to oestrogen-induced oxidative stress in a rat model of breast cancer [132], and a nested case—control study concluded that the long-term use of an oestrogen-based HRT was associated with an increased risk of suffering from breast cancer in postmenopausal women [133].

5. Conclusions

We reported here that the consumption of a blend of histidine, carnosine, cysteine and serine by a postmenopausal model with oestrogen deficiency, namely, OVX rats, decreased adiposity and RWAT adipocyte hypertrophy and improved body composition, as also evidenced by the increased lean body mass and lean/fat mass ratio. The decreases in the LAR and TC/HDL-c ratios and in the CRP plasma levels, as well as the favourable expression profile of key genes involved in the regulation of the cytoskeleton and ECM reorganization, glucose and insulin homeostasis, oxidative phosphorylation, cell fate determination and differentiation, inflammation and stress response found in the RWAT in response to MIS strongly suggest an improvement in immunometabolic health in OVX-MIS rats in response to MIS. To the best of our knowledge, this study is the first to report that the combination of these amino acid-related compounds exerted such effects. Our findings pave the way for promoting the use of this MIS formulation to ameliorate obesity and to improve the immunometabolic health of menopausal women. Further randomized controlled clinical trials performed with this target population treated with this MIS supplement are warranted.

Funding sources

This research was financially supported by the Agency for Business Competitiveness of the Government of Catalonia (ACCIÓ/TECCT11-1-0012) and by Comunidad de Madrid (S2022/BMD-7403 RENIM-CM).

CRediT authorship contribution statement

Francisca Mulero: Resources, Investigation, Funding acquisition. **Francesc Puiggròs:** Validation, Resources, Funding acquisition, Conceptualization. **Jordi Romero-Giménez:** Resources, Investigation. **Hong Yang:** Validation, Software, Resources, Methodology, Investigation, Formal analysis, Data curation. **Antoni Caimari:** Writing – review & editing, Validation, Supervision, Resources, Methodology, Funding acquisition, Conceptualization. **Adil Mardinoglu:** Validation, Resources, Conceptualization. **Lluís Arola:** Writing – review & editing, Validation, Supervision, Resources, Funding acquisition, Conceptualization. **Julia Hernandez-Baixauli:** Resources, Methodology, Investigation. **Julio Baudin:** Writing – review & editing, Writing – original draft, Visualization, Validation, Software, Resources, Methodology, Investigation, Formal analysis, Data curation, Conceptualization.

Declaration of Competing Interest

The authors declare that they have no known competing financial interests or personal relationships that could have appeared to influence the work reported in this paper.

Data Availability

Data will be made available on request.

Acknowledgements

Julio Baudin and Julia Hernandez-Baixauli were supported by a Vicente López fellowship (Eurecat).

We gratefully acknowledge the help from Dr. Juan Maria Alcaide-Hidalgo and Dr. Xavier Escoté, researchers at the Nutrition and Health Unit (Eurecat, Reus, Spain), who performed the study at the animal facility and performed the histological analyses in the RWAT, respectively. We also appreciate the assistance provided by Yaiza Tobajas, Anna Antolin, Cristina Egea and Gertruda Chomiciute, laboratory technicians at the Nutrition and Health Unit (Eurecat, Reus, Spain). The authors would like to thank the students Irene Bravo and David Sabador at the National Cancer Research Center (CNIO) for their support in the microcomputed tomography analyses.

Appendix A. Supporting information

Supplementary data associated with this article can be found in the online version at doi:10.1016/j.biopha.2024.117326.

References

[1] N. Santoro, J.F. Randolph, Reproductive hormones and the menopause transition, Obstet. Gynecol. Clin. North Am. 38 (2011) 455–466, https://doi.org/10.1016/j.ogc.2011.05.004.

[2] M.A. McNeil, S.B. Merriam, Menopause, Ann. Intern Med 174 (2021) ITC97–ITC112, https://doi.org/10.7326/AITC202107200.

[3] R.C. Thurston, B.D. Johnson, C.L. Shufelt, G.D. Braunstein, S.L. Berga, F. Z. Stanczyk, et al., Menopausal symptoms and cardiovascular disease mortality in the Women's ischemia syndrome evaluation (WISE), Menopause 24 (2017) 126–132, https://doi.org/10.1097/GME.0000000000000731.

[4] S. Thapa, A. Nandy, E. Rendina-Ruedy, Endocrinal metabolic regulation on the skeletal system in post-menopausal women, Front Physiol. 13 (2022) 1–10, https://doi.org/10.3389/fphys.2022.1052429.

[5] H. Juppi, S. Sipilä, V. Fachada, M. Hyvärinen, N. Cronin, P. Aukee, et al., Total and regional body adiposity increases during menopause—evidence from a follow-up study, Aging Cell 21 (2022) 1–17, https://doi.org/10.1111/acel.13621.

[6] M. Sowers, H. Zheng, K. Tomey, C. Karvonen-Gutierrez, M. Jannausch, X. Li, et al., Changes in body composition in women over six years at midlife: ovarian and chronological aging, J. Clin. Endocrinol. Metab. 92 (2007) 895–901, https://doi.org/10.1210/jc.2006-1393.

[7] S.H. Ko, H.S. Kim, Menopause-associated lipid metabolic disorders and foods beneficial for postmenopausal women, Nutrients 12 (2020) 202, https://doi.org/10.3390/nu12010202.

[8] O. Taleb-Belkadi, H. Chaib, L. Zemour, A. Fatah, B. Chafi, K. Mekki, Lipid profile, inflammation, and oxidative status in peri- and postmenopausal women, Gynecol. Endocrinol. 32 (2016) 982–985, https://doi.org/10.1080/09513590.2016.1214257.

[9] V.R. Mesch, L.E. Boero, N.O. Siseles, M. Royer, M. Prada, F. Sayegh, et al., Metabolic syndrome throughout the menopausal transition: influence of age and menopausal status, Climacteric 9 (2006) 40–48, https://doi.org/10.1080/13697130500487331.

[10] The European Society of Cardiology, Understanding the burden of CVD, 2023 https://www.escardio.org/The-ESC/Advocacy/understanding-the-burden-of-cvd-facts-and-figures (accessed September 2023).

[11] J. Mehta, J.M. Kling, J.E. Manson, Risks, benefits, and treatment modalities of menopausal hormone therapy: current concepts, Front Endocrinol. 26 (2021) 1–14, https://doi.org/10.3389/fendo.2021.564781.

[12] P. Thangavel, A. Puga-Olguín, J.F. Rodríguez-Landa, R.C. Zepeda, Genistein as potential therapeutic candidate for menopausal symptoms and other related diseases, Molecules 24 (2019) 3892, https://doi.org/10.3390/molecules24213892.

[13] A.M.P. Romani, The controversy on the beneficial effect of phytoestrogens in diabetic treatment in postmenopausal women, Biochem Pharm. 190 (2021) 114619, https://doi.org/10.1016/j.bcp.2021.114619.

[14] J. Baudin, J. Hernandez-Baixauli, S. Quesada-Vázquez, F. Mulero, F. Puiggròs, L. Arola, et al., Combined supplementation with hesperidin, phytosterols and curcumin decreases adiposity and improves metabolic health in ovariectomized rats, Food Funct. 15 (2024) 4905–4924, https://doi.org/10.1039/d3fo05122f.

[15] G. Frühbeck, V. Catalán, A. Rodríguez, B. Ramírez, S. Becerril, J. Salvador, et al., Adiponectin-leptin ratio is a functional biomarker of adipose tissue inflammation, Nutrients 11 (2019) 454, https://doi.org/10.3390/nu11020454.

[16] S. Quesada-Vázquez, A. Antolín, M. Colom-Pellicer, G. Aragonès, L. Herrero, J. M. Del Bas, et al., Reduction of obesity and insulin resistance through dual targeting of VAT and BAT by a novel combination of metabolic cofactors, Int J. Mol. Sci. 23 (2022) 14923, https://doi.org/10.3390/ijms232314923.

[17] J. Companys, L. Calderón-Pérez, L. Pla-Pagà, E. Llauradó, B.A. Sandoval-Ramirez, M.J. Gosalbes, et al., Effects of enriched seafood sticks (heat-inactivated B. animalis subsp. lactis CECT 8145, inulin, omega-3) on cardiometabolic risk factors and gut microbiota in abdominally obese subjects: randomized controlled trial, Eur. J. Nutr. 61 (2022) 3597–3611, https://doi.org/10.1007/s00394-022-02904-0.

[18] H. Yang, J. Mayneris-Perxachs, N. Boqué, J.M. del Bas, L. Arola, M. Yuan, et al., Combined metabolic activators decrease liver steatosis by activating mitochondrial metabolism in hamsters fed with a high-fat diet, Biomedicines 9 (2021) 1440, https://doi.org/10.3390/biomedicines9101440.

[19] S. Quesada-Vázquez, A. Castells-Nobau, J. Latorre, N. Oliveras-Cañellas, I. Puig-Parnau, N. Tejera, et al., Potential therapeutic implications of histidine catabolism by the gut microbiota in NAFLD patients with morbid obesity, Cell Rep. Med 4 (2023) 101341, https://doi.org/10.1016/j.xcrm.2023.101341.

[20] M. Suárez, N. Boqué, J. del Bas, J. Mayneris-Perxachs, L. Arola, A. Caimari, Mediterranean diet and multi-ingredient-based interventions for the management of non-alcoholic fatty liver disease, Nutrients 9 (2017) 1052, https://doi.org/10.3390/nu9101052.

[21] G. Caruso, L. Di Pietro, V. Cardaci, S. Maugeri, F. Caraci, The therapeutic potential of carnosine: focus on cellular and molecular mechanisms, Curr. Res Pharm. Drug Discov. 4 (2023) 100153, https://doi.org/10.1016/j.crphar.2023.100153.

[22] J.J. Matthews, E. Dolan, P.A. Swinton, L. Santos, G.G. Artioli, M.D. Turner, et al., Effect of carnosine or β-alanine supplementation on markers of glycemic control and insulin resistance in humans and animals: a systematic review and meta-analysis, Adv. Nutr. 12 (2021) 2216–2231, https://doi.org/10.1093/advances/nmab087.

[23] L. He, Y. Ding, X. Zhou, T. Li, Y. Yin, Serine signaling governs metabolic homeostasis and health, Trends Endocrinol. Metab. 34 (2023) 361–372, https://doi.org/10.1016/j.tem.2023.03.001.

[24] X. Zhou, H. Zhang, L. He, X. Wu, Y. Yin, Long-term l-serine administration reduces food intake and improves oxidative stress and Sirt1/NFκB signaling in the hypothalamus of aging mice, Front Endocrinol. 9 (2018) 476, https://doi.org/10.3389/fendo.2018.00476.

[25] S.K. Jain, P. Kanikarla-Marie, C. Warden, D. Micinski, L-cysteine supplementation upregulates glutathione (GSH) and vitamin D binding protein (VDBP) in hepatocytes cultured in high glucose and in vivo in liver, and increases blood levels of GSH, VDBP, and 25-hydroxy-vitamin D in Zucker diabetic fatty rats, Mol. Nutr. Food Res 60 (2016) 1090–1098, https://doi.org/10.1002/mnfr.201500667.

[26] S.K. Jain, T. Velusamy, J.L. Croad, J.L. Rains, R. Bull, l-Cysteine supplementation lowers blood glucose, glycated hemoglobin, CRP, MCP-1, and oxidative stress and inhibits NF-κB activation in the livers of Zucker diabetic rats, Free Radic. Biol. Med 46 (2009) 1633–1638, https://doi.org/10.1016/j.freeradbiomed.2009.03.014.

[27] A.E. Thalacker-Mercer, M.E. Gheller, Benefits and adverse effects of histidine supplementation, J. Nutr. 150 (2020) 2588S–2592S, https://doi.org/10.1093/jn/nxaa229.

[28] J. Moro, D. Tomé, P. Schmidely, T. chalvon Demersay, D. Azzout, Histidine: a systematic review on metabolism and physiological effects in human and different animal species, Nutrients 12 (2020) 1414, https://doi.org/10.3390/nu12051414, ut-marniche, histidine: a systematic review on metabolism and physiological effects in human and different animal speci.

[29] Y.C. Li, C.L. Li, J.Y. Qi, L.N. Huang, D. Shi, S.S. Du, et al., Relationships of dietary histidine and obesity in northern chinese adults, an internet-based cross-sectional study, Nutrients 8 (2016) 420, https://doi.org/10.3390/nu8070420.

[30] X. Sun, R. Feng, Y. Li, S. Lin, W. Zhang, Y. Li, et al., Histidine supplementation alleviates inflammation in the adipose tissue of high-fat diet-induced obese rats via the NF-κB- and PPARγ-involved pathways, Br. J. Nutr. 112 (2014) 477–485, https://doi.org/10.1017/S0007114514001056.

[31] R.N. Feng, Y.C. Niu, X.W. Sun, Q. Li, C. Zhao, C. Wang, et al., Histidine supplementation improves insulin resistance through suppressed inflammation in obese women with the metabolic syndrome: a randomised controlled trial, Diabetologia 56 (2013) 985–994, https://doi.org/10.1007/s00125-013-2839-7.

[32] D. Decandia, E. Landolfo, S. Sacchetti, F. Gelfo, L. Petrosini, D. Cutuli, n-3 PUFA improve emotion and cognition during menopause: a systematic review, Nutrients 14 (2022) 1982, https://doi.org/10.3390/nu14091982.

[33] T. Nakamura, F. Naganuma, U. Kudomi, S. Roh, K. Yanai, T. Yoshikawa, Oral histidine intake improves working memory through the activation of histaminergic nervous system in mice, Biochem Biophys. Res Commun. 609 (2022) 141–148, https://doi.org/10.1016/j.bbrc.2022.04.016.

[34] Y. Nozawa, M. Mimura, K. Yamada, M. Sugita, T. Shibakusa, N. Koyama, Dried bonito broth improves cognitive function via the histaminergic system in mice, Biomed. Res 35 (2014) 311–319, https://doi.org/10.2220/biomedres.35.311.

[35] S.F. Acevedo, T. Pfankuch, H. Ohtsu, J. Raber, Anxiety and cognition in female histidine decarboxylase knockout (Hdc -/-) mice, Behav. Brain Res 168 (2006) 92–99, https://doi.org/10.1016/j.bbr.2005.10.016.

[36] S.F. Acevedo, H. Ohtsu, T.S. Benice, A. Rizk-Jackson, J. Raber, Age-dependent measures of anxiety and cognition in male histidine decarboxylase knockout (Hdc-/-) mice, Brain Res. 1071 (2006) 113–123, https://doi.org/10.1016/j.brainres.2005.11.067.

[37] S. Tomonaga, H. Yamane, E. Onitsuka, S. Yamada, M. Sato, Y. Takahata, et al., Carnosine-induced antidepressant-like activity in rats, Pharm. Biochem Behav. 89 (2008) 627–632, https://doi.org/10.1016/j.pbb.2008.02.021.

[38] Y.F. Li, R.R. He, B. Tsoi, X.D. Li, W.X. Li, K. Abe, et al., Anti-Stress Effects of Carnosine on Restraint-Evoked Immunocompromise in Mice through Spleen Lymphocyte Number Maintenance. Frasch MG, editor, PLoS One 7 (2012) e33190, https://doi.org/10.1371/journal.pone.0033190.

[39] B. Araminia, M. Shalbafan, A. Mortezaei, E. Shirazi, S. Ghaffari, E. Sahebolzamani, et al., L-Carnosine combination therapy for major depressive disorder: a randomized, double-blind, placebo-controlled trial, J. Affect Disord. 267 (2020) 131–136, https://doi.org/10.1016/j.jad.2020.02.020.

[40] A.K. Elshorbagy, C.G. Gjesdal, E. Nurk, G.S. Tell, P.M. Ueland, O. Nygård, et al., Cysteine, homocysteine and bone mineral density: a role for body composition? Bone 44 (2009) 954–958, https://doi.org/10.1016/j.bone.2008.12.018.

[41] M. Baines, M.B. Kredan, A. Davison, G. Higgins, C. West, W.D. Fraser, et al., The Association between cysteine, bone turnover, and low bone mass, Calcif. Tissue Int 81 (2007) 450–454, https://doi.org/10.1007/s00223-007-9089-y.

[42] N.R. Han, N.R. Kim, H.M. Kim, H.J. Jeong, Cysteine Prevents Menopausal Syndromes in Ovariectomized Mouse, Reprod. Sci. 23 (2016) 670–679, https://doi.org/10.1177/1933719115612133.

[43] S. Reagan-Shaw, M. Nihal, N. Ahmad, Dose translation from animal to human studies revisited, FASEB J. 22 (2008) 659–661, https://doi.org/10.1096/fj.07-9574LSF.

[44] A. Mardinoglu, D. Ural, M. Zeybel, H.H. Yuksel, M. Uhlén, J. Borén, The Potential Use of Metabolic Cofactors in Treatment of NAFLD, Nutrients 11 (2019) 1578, https://doi.org/10.3390/nu11071578.

[45] M. Holeček, Side effects of amino acid supplements, Physiol. Res 71 (2022) 29–45, https://doi.org/10.33549/physiolres.934790.

[46] W. Dröge, Oxidative stress and ageing: is ageing a cysteine deficiency syndrome? Philos. Trans. R. Soc. B Biol. Sci. 360 (2005) 2355–2372, https://doi.org/10.1098/rstb.2005.1770.

[47] D.R. Matthews, J.P. Hosker, A.S. Rudenski, B.A. Naylor, D.F. Treacher, R. C. Turner, Homeostasis model assessment: insulin resistance and beta-cell function from fasting plasma glucose and insulin concentrations in man, Diabetologia 28 (1985) 412–419, https://doi.org/10.1007/BF00280883.

[48] P. López-Jaramillo, D. Gómez-Arbeláez, J. López-López, C. López-López, J. Martínez-Ortega, A. Gómez-Rodríguez, et al., The role of leptin/adiponectin ratio in metabolic syndrome and diabetes, Horm. Mol. Biol. Clin. Invest. 18 (2014) 37–45, https://doi.org/10.1515/hmbci-2013-0053.

[49] A. Crescenti, J.M. del Bas, A. Arola-Arnal, G. Oms-Oliu, L. Arola, A. Caimari, Grape seed procyanidins administered at physiological doses to rats during pregnancy and lactation promote lipid oxidation and up-regulate AMPK in the muscle of male offspring in adulthood, J. Nutr. Biochem 26 (2015) 912–920, https://doi.org/10.1016/j.jnutbio.2015.03.003.

[50] A.K. Kraeuter, P.C. Guest, Z. Sarnyai, The Elevated Plus Maze Test for Measuring Anxiety-Like Behavior in Rodents, in: Methods in molecular biology, 2nd edit., vol. 1916, Springer, New York, 2019, pp. 69–74, https://doi.org/10.1007/978-1-4939-8994-2_4.

[51] R.J. Rodgers, N.J.T. Johnson, Factor analysis of spatiotemporal and ethological measures in the murine elevated plus-maze test of anxiety, Pharm. Biochem Behav. 52 (1995) 297–303, https://doi.org/10.1016/0091-3057(95)00138-m.

[52] S. Pellow, P. Chopin, S.E. File, M. Briley, Validation of open: closed arm entries in an elevated plus-maze as a measure of anxiety in the rat, J. Neurosci. Methods 14 (1985) 149–167, https://doi.org/10.1016/0165-0270(85)90031-7.

[53] G.R. Dawson, M.D. Tricklebank, Use of the elevated plus maze in the search for novel anxiolytic agents, Trends Pharm. Sci. 16 (1995) 33–36, https://doi.org/10.1016/s0165-6147(00)88973-7.

[54] A.K. Kraeuter, P.C. Guest, Z. Sarnyai, The Y-Maze for Assessment of Spatial Working and Reference Memory in Mice, in: P.C. Guest (Ed.), in *Methods in molecular biology*, vol. 1916, Springer, New York, 2019, pp. 105–111, https://doi.org/10.1007/978-1-4939-8994-2_10.

[55] M.I. Love, W. Huber, S. Anders, Moderated estimation of fold change and dispersion for RNA-seq data with DESeq2, Genome Biol. 15 (2014) 550, https://doi.org/10.1186/s13059-014-0550-8.

[56] L. Väremo, J. Nielsen, I. Nookaew, Enriching the gene set analysis of genome-wide data by incorporating directionality of gene expression and combining statistical hypotheses and methods, Nucleic Acids Res 41 (2013) 4378–4391, https://doi.org/10.1093/nar/gkt111.

[57] Z. Gu, R. Eils, M. Schlesner, Complex heatmaps reveal patterns and correlations in multidimensional genomic data, Bioinformatics 32 (2016) 2847–2849, https://doi.org/10.1093/bioinformatics/btw313.

[58] H. Wickham, "Ggplot2: Elegant Graphics for Data Analysis", in: R. Gentleman, K. Hornik, G. Parmigian (Eds.), *Use R!*, ed., Springer, Switzerland, 2016 https://doi.org/10.1007/978-3-319-24277-4.

[59] L. Kolberg, U. Raudvere, I. Kuzmin, P. Adler, J. Vilo, H. Peterson, g: Profiler—interoperable web service for functional enrichment analysis and gene identifier mapping (2023 update), Nucleic Acids Res 51 (2023) W207–W212, https://doi.org/10.1093/nar/gkad347.

[60] A. Valavanidis, T. Vlachogianni, C. Fiotakis, 8-hydroxy-2′ -deoxyguanosine (8-OHdG): A Critical Biomarker of Oxidative Stress and Carcinogenesis, J. Environ. Sci. Heal Part C. 27 (2009) 120–139, https://doi.org/10.1074/jbc.M110.103713.

[61] J. Medina-Contreras, R. Villalobos-Molina, A. Zarain-Herzberg, J. Balderas-Villalobos, Ovariectomized rodents as a menopausal metabolic syndrome model. A minireview, Mol. Cell Biochem 475 (2020) 261–276, https://doi.org/10.1007/s11010-020-03879-4.

[62] N. Yousefzadeh, K. Kashfi, S. Jeddi, A. Ghasemi, Ovariectomized rat model of osteoporosis: a practical guide, EXCLI J. 19 (2020) 89–107, https://doi.org/10.17179/excli2019-1990.

[63] S. Kasaoka, Y. Kawahara, S. Inoue, M. Tsuji, H. Kato, T. Tsuchiya, et al., Gender effects in dietary histidine-induced anorexia, Nutrition 21 (2005) 855–858, https://doi.org/10.1016/j.nut.2004.12.009.

[64] K.M. Gavin, W.M. Kohrt, D.J. Klemm, E.L. Melanson, Modulation of energy expenditure by estrogens and exercise in women, Exerc Sport Sci. Rev. 46 (2018) 232–239, https://doi.org/10.1249/JES.0000000000000160.

[65] J.C. Lovejoy, C.M. Champagne, L. de Jonge, H. Xie, S.R. Smith, Increased visceral fat and decreased energy expenditure during the menopausal transition, Int J. Obes. 32 (2008) 949–958, https://doi.org/10.1038/ijo.2008.25.

[66] S. Kasaoka, N. Tsuboyama-Kasaoka, Y. Kawahara, S. Inoue, M. Tsuji, O. Ezaki, et al., Histidine supplementation suppresses food intake and fat accumulation in rats, Nutrition 20 (2004) 991–996, https://doi.org/10.1016/j.nut.2004.08.006.

[67] R. Asahi, K. Tanaka, T.J. Fujimi, N. Kanzawa, S. Nakajima, Proline decreases the suppressive effect of histidine on food intake and fat accumulation, J. Nutr. Sci. Vitam. 62 (2016) 277–280, https://doi.org/10.3177/jnsv.62.277.

[68] E. López-Gonzales, L. Lehmann, F.J. Ruiz-Ojeda, R. Hernández-Bautista, I. Altun, Y. Onogi, et al., L-serine supplementation blunts fasting-induced weight regain by increasing brown fat thermogenesis, Nutrients 14 (2022) 1922, 10.3390/nu14091922. .

[69] M.C. Hunt, M.I. Siponen, S.E.H. Alexson, The emerging role of acyl-CoA thioesterases and acyltransferases in regulating peroxisomal lipid metabolism, Biochim Biophys. Acta - Mol. Basis Dis. 1822 (2012) 1397–1410, https://doi.org/10.1016/j.bbadis.2012.03.009.

[70] Y.Q. Liang, M. Akishita, S. Kim, J. Ako, M. Hashimoto, K. Iijima, et al., Estrogen receptor β is involved in the anorectic action of estrogen, Int J. Obes. 26 (2002) 1103–1109, https://doi.org/10.1038/sj.ijo.0802054.

[71] G.Z. Taicher, F.C. Tinsley, A. Reiderman, M.L. Heiman, Quantitative magnetic resonance (QMR) method for bone and whole-body-composition analysis, Anal. Bioanal. Chem. 377 (2003) 990–1002, https://doi.org/10.1007/s00216-003-2224-3.

[72] N. López, J. Sánchez, C. Picó, A. Palou, F. Serra, Dietary l-leucine supplementation of lactating rats results in a tendency to increase lean/fat ratio associated to lower orexigenic neuropeptide expression in hypothalamus, Peptides 31 (7) (2010) 1361, https://doi.org/10.1016/j.peptides.2010.03.028.

[73] C. Hepler, J. Bass, Circadian mechanisms in adipose tissue bioenergetics and plasticity, Genes Dev. 37 (2023) 454–473, https://doi.org/10.1101/gad.350759.123.

[74] A. Charrier, X. Xu, B.J. Guan, J. Ngo, A. Wynshaw-Boris, M. Hatzoglou, et al., Adipocyte-specific deletion of zinc finger protein 407 results in lipodystrophy and insulin resistance in mice, Mol. Cell Endocrinol. 521 (2021) 111109, https://doi.org/10.1016/j.mce.2020.111109.

[75] J. Tian, H.N. Dang, J. Yong, W.S. Chui, M.P.G. Dizon, C.K.Y. Yaw, et al., Oral Treatment with γ-aminobutyric acid improves glucose tolerance and insulin sensitivity by inhibiting inflammation in high fat diet-fed mice, PLoS One 6 (2011) 25338, https://doi.org/10.1371/journal.pone.0025338.

[76] Z. Heli, C. Hongyu, B. Dapeng, T. Yee Shin, Z. Yejun, Z. Xi, et al., Recent advances of γ-aminobutyric acid: physiological and immunity function, enrichment, and metabolic pathway, Front Nutr. 9 (2022) 1–16, https://doi.org/10.3389/fnut.2022.1076223.

[77] E. Conceição-Furber, T. Coskun, K.W. Sloop, R.J. Samms, Is glucagon receptor activation the thermogenic solution for treating obesity? Front Endocrinol. 13 (2022) 1–9, https://doi.org/10.3389/fendo.2022.868037.

[78] M.J. Pereira, K. Thombare, A. Sarsenbayeva, P.G. Kamble, K. Almby, M. Lundqvist, et al., Direct effects of glucagon on glucose uptake and lipolysis in human adipocytes, Mol. Cell Endocrinol. 503 (2020) 110696, https://doi.org/10.1016/j.mce.2019.110696.

[79] D. Schleinitz, N. Klöting, C.M. Lindgren, J. Breitfeld, A. Dietrich, M.R. Schön, et al., Fat depot-specific mRNA expression of novel loci associated with waist–hip ratio, Int J. Obes. 38 (2014) 120–125, https://doi.org/10.1038/ijo.2013.56.

[80] B. Cariou, N. Capitaine, V. Le Marcis, N. Vega, V. Bériziat, M. Kergoat, et al., Increased adipose tissue expression of Grb14 in several models of insulin resistance, FASEB J. 18 (2004) 965–967, https://doi.org/10.1096/fj.03-0824fje.

[81] C. Sun, F. Förster, B. Gutsmann, Y. Moulla, C. Stroh, A. Dietrich, et al., Metabolic effects of the waist-to-hip ratio associated locus GRB14/COBLL1 are related to GRB14 expression in adipose tissue, Int J. Mol. Sci. 23 (2022) 8558, https://doi.org/10.3390/ijms23158558.

[82] T. Khan, E.S. Muise, P. Iyengar, Z.V. Wang, M. Chandalia, N. Abate, et al., Metabolic dysregulation and adipose tissue fibrosis: role of collagen VI, Mol. Cell Biol. 29 (2009) 1575–1591, https://doi.org/10.1128/MCB.01300-08.

[83] A. Munoz, N. Abate, M. Chandalia, Adipose tissue collagen and inflammation in nonobese Asian Indian men, J. Clin. Endocrinol. Metab. 98 (2013) E1360–E1363, https://doi.org/10.1210/jc.2012-3841.

[84] T.H. Chun, Peri-adipocyte ECM remodeling in obesity and adipose tissue fibrosis, Adipocyte 1 (2012) 89–95, https://doi.org/10.4161/adip.19752.

[85] Y. Zhao, Z. Yu, Y. Song, L. Fan, T. Lei, Y. He, et al., The regulatory network of CREB3L1 and its roles in physiological and pathological conditions, Int J. Med Sci. 21 (2024) 123–136, https://doi.org/10.7150/ijms.90189.

[86] A. Huang, Y. Lin, L. Kao, Y. Chiou, G. Lee, H. Lin, et al., Inflammation-induced macrophage lysyl oxidase in adipose stiffening and dysfunction in obesity, Clin. Transl. Med 11 (2021) 2–8, https://doi.org/10.1002/ctm2.543.

[87] M. Soták, M.R. Rajan, M. Clark, C. Biörserud, V. Wallenius, C.E. Hagberg, et al., Healthy subcutaneous and omental adipose tissue is associated with high expression of extracellular matrix components, Int J. Mol. Sci. 23 (2022) 520, https://doi.org/10.3390/ijms23010520.

[88] B. Meissburger, L. Stachorski, E. Röder, G. Rudofsky, C. Wolfrum, Tissue inhibitor of matrix metalloproteinase 1 (TIMP1) controls adipogenesis in obesity in mice and in humans, Diabetologia 54 (2011) 1468–1479, https://doi.org/10.1007/s00125-011-2093-9.

[89] E. Maquoi, C. Munaut, A. Colige, D. Collen, H.R. Lijnen, Modulation of adipose tissue expression of murine matrix metalloproteinases and their tissue inhibitors with obesity, Diabetes 51 (2002) 1093–1101, https://doi.org/10.2337/diabetes.51.4.1093.

[90] Y. Ren, H. Zhao, C. Yin, X. Lan, L. Wu, X. Du, et al., Adipokines, hepatokines and myokines: focus on their role and molecular mechanisms in adipose tissue inflammation, Front Endocrinol. 13 (2022) 1–26, https://doi.org/10.3389/fendo.2022.873699.

[91] M. Takahashi, H. Nagaretani, T. Funahashi, H. Nishizawa, N. Maeda, K. Kishida, et al., The expression of SPARc in adipose tissue and its increased plasma concentration in patients with coronary artery disease, Obes. Res 9 (2001) 388–393, https://doi.org/10.1038/oby.2001.50.

[92] S.H. Lee, J.A. Lee, H.S. Park, Y.S. Song, Y.J. Jang, J.H. Kim, et al., Associations among SPARC mRNA expression in adipose tissue, serum SPARC concentration and metabolic parameters in Korean women, Obesity 21 (2013) 2296–2302, https://doi.org/10.1002/oby.20183.

[93] J. Kim, S.K. Lee, J. min Shin, U. woo Jeoun, Y.J. Jang, H.S. Park, et al., Enhanced biglycan gene expression in the adipose tissues of obese women and its association with obesity-related genes and metabolic parameters, Sci. Rep. 6 (2016) 30609, https://doi.org/10.1038/srep30609.

[94] J. Shin, S. Toyoda, Y. Okuno, R. Hayashi, S. Nishitani, T. Onodera, et al., HSP47 levels determine the degree of body adiposity, Nat. Commun. 14 (2023) 7319, https://doi.org/10.1038/s41467-023-43080-x.

[95] D.B. Ballak, R. Stienstra, C.J. Tack, C.A. Dinarello, J.A. van Diepen, IL-1 family members in the pathogenesis and treatment of metabolic disease: Focus on adipose tissue inflammation and insulin resistance, Cytokine 75 (2015) 280–290, https://doi.org/10.1016/j.cyto.2015.05.005.

[96] M. Blüher, N. Klöting, S. Wueest, E.J. Schoenle, M.R. Schön, A. Dietrich, et al., Fas and FasL expression in human adipose tissue is related to obesity, insulin resistance, and type 2 diabetes, J. Clin. Endocrinol. Metab. 99 (2014) E36–E44, https://doi.org/10.1210/jc.2013-2488.

[97] C. Rouault, V. Pellegrinelli, R. Schilch, A. Cotillard, C. Poitou, J. Tordjman, et al., Roles of chemokine ligand-2 (CXCL2) and neutrophils in influencing endothelial cell function and inflammation of human adipose tissue, Endocrinology 154 (2013) 1069–1079, https://doi.org/10.1210/en.2012-1415.

[98] J. Hellmann, B.E. Sansbury, C.R. Holden, Y. Tang, B. Wong, M. Wysoczynski, et al., CCR7 maintains nonresolving lymph node and adipose inflammation in obesity, Diabetes 65 (2016) 2268–2281, https://doi.org/10.2337/db15-1689.

[99] Y. Pan, S. Cao, J. Tang, J.P. Arroyo, A.S. Terker, Y. Wang, et al., Cyclooxygenase-2 in adipose tissue macrophages limits adipose tissue dysfunction in obese mice, J. Clin. Invest 132 (2022) e152391, https://doi.org/10.1172/JCI1523912.
[100] L. Wang, Y. Wang, C. Zhang, J. Li, Y. Meng, M. Dou, et al., Inhibiting glycogen synthase kinase 3 reverses obesity-induced white adipose tissue inflammation by regulating apoptosis inhibitor of macrophage/cd5l-mediated macrophage migration, Arterioscler. Thromb. Vasc. Biol. 38 (2018) 2103–2116, https://doi.org/10.1161/ATVBAHA.118.311363.
[101] G.S.D. Purvis, M. Collino, H. Aranda-Tavio, F. Chiazza, C.E. O'Riordan, L. Zeboudj, et al., Inhibition of Bruton's TK regulates macrophage NF-κB and NLRP3 inflammasome activation in metabolic inflammation, Br. J. Pharm. 177 (2020) 4416–4432, https://doi.org/10.1111/bph.15182.
[102] G.S.D. Purvis, M. Collino, A.D. van Dam, G. Einaudi, Y. Ng, M. Shanmuganathan, et al., OxPhos in adipose tissue macrophages regulated by BTK enhances their M2-like phenotype and confers a systemic immunometabolic benefit in obesity, Diabetes (2024) 1–50, https://doi.org/10.2337/db22-0275.
[103] J. Nie, E.H. Sage, SPARC Inhibits adipogenesis by its enhancement of β-catenin signaling, J. Biol. Chem. 284 (2009) 1279–1290, https://doi.org/10.1074/jbc.M808285200.
[104] L. Wang, C. guang Zhang, Y. lin Jia, L. Hu, Tissue inhibitor of metalloprotease-1 (TIMP-1) regulates adipogenesis of adipose-derived stem cells (ASCs) via the Wnt signaling pathway in an MMP-independent manner, Curr. Med Sci. 40 (2020) 989–996, https://doi.org/10.1007/s11596-020-2265-2.
[105] A. Hammarstedt, S. Hedjazifar, L. Jenndahl, S. Gogg, J. Grünberg, B. Gustafson, et al., WISP2 regulates preadipocyte commitment and PPARγ activation by BMP4, Proc. Natl. Acad. Sci. 110 (2013) 2563–2568, https://doi.org/10.1073/pnas.1211255110.
[106] H.S. Shitaye, S.P. Terkhorn, J.A. Combs, K.D. Hankenson, Thrombospondin-2 is an endogenous adipocyte inhibitor, Matrix Biol. 29 (2010) 549–556, https://doi.org/10.1016/j.matbio.2010.05.006.
[107] M.K. Jang, C.H. Kim, J.K. Seong, M.H. Jung, ATF3 inhibits adipocyte differentiation of 3T3-L1 cells, Biochem Biophys. Res Commun. 421 (2012) 38–43, https://doi.org/10.1016/j.bbrc.2012.03.104.
[108] K.B. Boyle, D. Hadaschik, S. Virtue, W.P. Cawthorn, S.H. Ridley, S. O'Rahilly, et al., The transcription factors Egr1 and Egr2 have opposing influences on adipocyte differentiation, Cell Death Differ. (16) (2009) 782–789, https://doi.org/10.1016/j.bbrc.2012.03.104.
[109] Y.M. Park, Y. ho Lee, S.H. Kim, E.Y. Lee, K.S. Kim, D.R. Williams, et al., Snail, a transcriptional regulator, represses adiponectin expression by directly binding to an E-box motif in the promoter, Metabolism 61 (2012) 1622–1632, https://doi.org/10.1016/j.metabol.2012.04.014.
[110] J. Hino, T. Miyazawa, M. Miyazato, K. Kangawa, Bone morphogenetic protein-3b (BMP-3b) is expressed in adipocytes and inhibits adipogenesis as a unique complex, Int J. Obes. 36 (2012) 725–734, https://doi.org/10.1038/ijo.2011.124.
[111] S.C. Butterwith, Molecular events in adipocyte development, Pharm. Ther. 61 (1994) 399–411, https://doi.org/10.1016/0163-7258(94)90018-3.
[112] Y. Zhao, Y.D. Zhang, Y.Y. Zhang, S.W. Qian, Z.C. Zhang, S.F. Li, et al., p300-Dependent acetylation of activating transcription factor 5 enhances C/EBPβ transactivation of C/EBPα during 3T3-L1 differentiation, Mol. Cell Biol. 34 (2014) 315–324, https://doi.org/10.1128/MCB.00956-13.
[113] H. Zhang, X. Chen, M.R. Sairam, Novel genes of visceral adiposity: identification of mouse and human mesenteric estrogen-dependent adipose (MEDA)-4 gene and its adipogenic function, Endocrinology 153 (2012) 2665–2676, https://doi.org/10.1210/en.2011-2008.
[114] X. Liu, H. Li, L. Zhang, L. Wang, L. Wang, Expression and genetic effects of GLI pathogenesis-related 1 gene on backfat thickness in pigs, Genes 13 (2022) 1448, https://doi.org/0.3390/genes13081448.
[115] A. Ehrlund, N. Mejhert, S. Lorente-Cebrián, G. Åström, I. Dahlman, J. Laurencikiene, et al., Characterization of the Wnt inhibitors secreted frizzled-related proteins (SFRPs) in human adipose tissue, J. Clin. Endocrinol. Metab. 98 (2013) E503–E508, https://doi.org/10.1210/jc.2012-3416.
[116] E. Guiu-Jurado, M. Unthan, N. Böhler, M. Kern, K. Landgraf, A. Dietrich, et al., Bone morphogenetic protein 2 (BMP2) may contribute to partition of energy storage into visceral and subcutaneous fat depots, Obesity 24 (2016) 2092–2100, https://doi.org/10.1002/oby.21571.
[117] G. Ren, C. Beech, C.M. Smas, The immunoglobulin Superfamily protein differentiation of embryonic stem cells 1 (Dies1) has a regulatory role in preadipocyte to adipocyte conversion, in: M. Vinciguerra (Ed.), PLoS One, **8**, 2013 e65531, https://doi.org/10.1371/journal.pone.0065531.
[118] C.S. Hudak, H.S. Sul, Pref-1, a gatekeeper of adipogenesis, Front Endocrinol. 4 (2013) 1–6, https://doi.org/10.3389/fendo.2013.00079.
[119] X. Yu, N. Shen, M.L. Zhang, F.Y. Pan, C. Wang, W.P. Jia, et al., Egr-1 decreases adipocyte insulin sensitivity by tilting PI3K/Akt and MAPK signal balance in mice, EMBO J. 30 (2011) 3754–3765, https://doi.org/10.1038/emboj.2011.277.
[120] Y. Hua, D. Xie, Y. Zhang, M. Wang, W. Wen, J. Sun, Identification and analysis of key genes in adipose tissue for human obesity based on bioinformatics, Gene 888 (2023) 147755, https://doi.org/10.1016/j.gene.2023.147755.
[121] D. Favre, E. Le Gouill, D. Fahmi, C. Verdumo, G. Chinetti-Gbaguidi, B. Staels, et al., Impaired expression of the inducible cAMP early repressor accounts for sustained adipose CREB activity in obesity, Diabetes 60 (2011) 3169–3174, https://doi.org/10.2337/db10-1743.
[122] X. Zhang, Z. Liu, W. Li, Y. Kang, Z. Xu, X. Li, et al., MAPKs/AP-1, not NF-κB, is responsible for MCP-1 production in TNF-α-activated adipocytes, Adipocyte 11 (2022) 477–486, https://doi.org/10.1080/21623945.2022.2107786.
[123] S. Bahrami, F. Drabløs, Gene regulation in the immediate-early response process, Adv. Biol. Regul. 62 (2016) 37–49, https://doi.org/10.1016/j.jbior.2016.05.001.
[124] S.N. Dankel, D.J. Fadnes, A.K. Stavrum, C. Stansberg, R. Holdhus, T. Hoang, et al., Switch from stress response to homeobox transcription factors in adipose tissue after profound fat loss, in: T.I.A. Sorensen (Ed.), PLoS One, **5**, 2010 e11033, https://doi.org/10.1371/journal.pone.0011033.
[125] R. Schübel, D. Sookthai, J. Greimel, T. Johnson, M. Grafetstätter, R. Kirsten, et al., Key genes of lipid metabolism and WNT-signaling are downregulated in subcutaneous adipose tissue with moderate weight loss, Nutrients 11 (2019) 639, https://doi.org/10.3390/nu11030639.
[126] M. Gaggini, F. Gorini, C. Vassalle, Lipids in atherosclerosis: pathophysiology and the role of calculated lipid indices in assessing cardiovascular risk in patients with hyperlipidemia, Int J. Mol. Sci. 24 (2022) 75, https://doi.org/10.3390/ijms24010075.
[127] J. Feehan, R. Hariharan, T. Buckenham, C. Handley, A. Bhatnagar, S.P. Baba, et al., Carnosine as a potential therapeutic for the management of peripheral vascular disease, Nutr. Metab. Cardiovasc Dis. 32 (2022) 2289–2296, https://doi.org/10.1016/j.numecd.2022.07.006.
[128] N.A. Al-Sawalha, O.Y. Alshogran, M.S. Awawdeh, B.A. Almomani, The effects of L-Carnosine on development of metabolic syndrome in rats, Life Sci. 237 (2019), https://doi.org/10.1016/j.lfs.2019.116905.
[129] R. Takanabe-Mori, K. Ono, N. Sowa, H. Wada, T. Takaya, T. Horie, et al., Lectin-like oxidized low-density lipoprotein receptor-1 is required for the adipose tissue expression of proinflammatory cytokines in high-fat diet-induced obese mice, Biochem Biophys. Res Commun. 398 (2010) 576–580, https://doi.org/10.1016/j.bbrc.2010.06.123.
[130] T.E. Brinkley, N. Kume, H. Mitsuoka, D.A. Phares, J.M. Hagberg, Elevated soluble lectin-like oxidized LDL Receptor-1 (sLOX-1) levels in obese postmenopausal women, Obesity 16 (6) (2008) 1454, https://doi.org/10.1038/oby.2008.213.
[131] M. Zeybel, O. Altay, M. Arif, X. Li, H. Yang, C. Fredolini, et al., Combined metabolic activators therapy ameliorates liver fat in nonalcoholic fatty liver disease patients, Mol. Syst. Biol. 17 (2021) 1–18, https://doi.org/10.15252/msb.202110459.
[132] B. Singh, N.K. Bhat, H.K. Bhat, Induction of NAD(P)H-quinone oxidoreductase 1 by antioxidants in female ACI rats is associated with decrease in oxidative DNA damage and inhibition of estrogen-induced breast cancer, Carcinogenesis 33 (2012) 156–163, https://doi.org/10.1093/carcin/bgr237.
[133] C.L. Chen, Hormone replacement therapy in relation to breast cancer, JAMA 287 (2002) 734–741, https://doi.org/10.1001/jama.287.6.734.